LAWRENCE
LIVERMORE
NATIONAL
LABORATORY

LLNL-TR-663374

Background Information for Independent Review Team: Lifecycle Plan and FY14 Quarterly Reports

V. Lordi

October 27, 2014

Disclaimer

This document was prepared as an account of work sponsored by an agency of the United States government. Neither the United States government nor Lawrence Livermore National Security, LLC, nor any of their employees makes any warranty, expressed or implied, or assumes any legal liability or responsibility for the accuracy, completeness, or usefulness of any information, apparatus, product, or process disclosed, or represents that its use would not infringe privately owned rights. Reference herein to any specific commercial product, process, or service by trade name, trademark, manufacturer, or otherwise does not necessarily constitute or imply its endorsement, recommendation, or favoring by the United States government or Lawrence Livermore National Security, LLC. The views and opinions of authors expressed herein do not necessarily state or reflect those of the United States government or Lawrence Livermore National Security, LLC, and shall not be used for advertising or product endorsement purposes.

This work performed under the auspices of the U.S. Department of Energy by Lawrence Livermore National Laboratory under Contract DE-AC52-07NA27344.

Office of Nonproliferation and Verification R&D (NA-22)
Defense Nuclear Nonproliferation (NA-20)
National Nuclear Security Administration

FY2013 PROJECT LIFECYCLE PLAN – REVISION

Date:	September 13, 2013
Title:	**Materials Modeling for High-Performance Radiation Detectors**
WebPMIS Project #:	LL13-MatModelRadDetect-PD3YJ
Lead Principal Investigator:	Vincenzo Lordi, 925-423-2755, lordi2@llnl.gov Lawrence Livermore National Laboratory
Co-Investigator(s):	N. Adelstein (PD), 925-422-3969, adelstein1@llnl.gov Donghwa Lee (PD), 925-423-5028, lee1004@llnl.gov Daniel Åberg, 925-423-0896, aberg2@llnl.gov Vasily Bulotov, 925-423-0124, bulatov1@llnl.gov
NA22 Programmatic Area:	NN2001-05 Program Name: Advanced Materials Program Manager: David Beach

DESCRIPTION OF PROJECT

This project is in collaboration with SL13-FY13-237-PD05. This project aims to enable rational materials design for select high-payoff challenges in radiation detection materials by using state-of-the-art modeling techniques bridging multiple resolutions, in cooperation with experimental collaborations. Three specific high-impact challenges are addressed: design of contacts for TlBr detectors to stabilize response at room-temperature; design of host glass for large-volume, low-cost, high-performance scintillators; and determination of the electrical impacts of dislocation networks in CZT that limit the performance and usable single-crystal volume. The realization of these goals will impact a number of proliferation detection application areas, including improved-performance and reduced-cost handheld detectors for search- and contain-missions (TlBr and CZT), and large-volume, specially-shaped detectors for portal monitors, tracking detectors, and similar applications (glass scintillators). The direct products of this project will be design and process strategies to achieve improved materials, whose implementation will yield detector devices that meet mission objectives. An added value of this project will be further advancement of the state-of-the-art in materials design capabilities, which is broadly useful for future materials needs.

LCP TABLE OF CONTENTS

Objective 2
Application 3
Users 3
Researchers 3
Prior Work 6
Collaborators 9
Work for Others 10
Proposed Work and Scientific Basis 10
Technical Issues 14
References 15

PROJECT NARRATIVE

OBJECTIVE

The main objective of this project is to enable rational materials design for select high-payoff challenges in radiation detection materials by using state-of-the-art materials modeling techniques that bridge multiple scales. Three specific challenges are targeted, balancing near-term needs with higher-risk longer-term research, building upon our team's prior work on computational materials optimization of radiation detection materials for more than 6 years. Our computational work will, as in the past, couple with experimental efforts across industry and national laboratories to remain relevant and impact real materials development.

The three foci of the proposed work are: (i) optimization of material selection for the electrical contact interfaces of TlBr detectors to produce temporally stable detectors at room temperature; (ii) exploration of carrier transport and electronic states in host materials of glass scintillators, to relate local structural dispersions from composition and process variations and to enable high-performance glass scintillators; and (iii) determination of the electronic properties (carrier trapping) of dislocation networks in CdTe/CZT. TlBr detectors show great promise for high-resolution room-temperature detectors, but temporal decay of their performance (often termed "polarization") have stymied practical implementation; recent results by our collaborators and ourselves have indicated that the contact interfaces are the dominant remaining contribution to detector instabilities. Glass scintillators may hold great promise for low-cost, large-volume, formable detectors; however, the light yield and resolution of current materials have been more than an order of magnitude worse than crystalline scintillators and far from the theoretical limits. Fundamental understanding of carrier transport and limits on activator loading of different glass hosts is lacking and is essential to designing high-performance glass scintillators. Finally, CZT is the most mature room-temperature gamma radiation detector material, but high-yield growth of large uniform crystals with spectroscopic quality remains problematic. One of the remaining unknowns affecting performance is the electrical impact of dislocation networks in the material, namely how dislocations and associated structures capture carriers and reduce their lifetimes. In particular, we aim to understand the role of dislocation networks on carrier capture, and whether impurities or precipitates that are often observed to decorate the dislocations are the true culprits.

All three aspects of the proposed project will build upon previous work by our team and also bridge multiple scales in length, time, and detail of the physical models—from quantum mechanical to semi-empirical and continuum models. The result will be multi-resolution modeling of "real" materials to enable advances in critical challenges for radiation detection materials.

APPLICATION

The high value products of this project will be the realization of improved radiation detection materials to help meet the performance and operational goals of the proliferation detection mission. The achievement of temporally-stable, high-resolution TlBr radiation detectors operating at room-temperature would provide gamma spectroscopy suitable for identifying isotopes rapidly for both the search- and contain-missions. These may find the most use in the near-term in handheld isotope identifiers; however, if larger, less expensive crystals are available in the future, additional applications can be imagined as well. Similarly, improved growth of larger, high-performance single crystals of CZT in a cost effective manner would have similarly high impact and applications. The main hurdle for CZT is to understand and circumvent the problems with growing large single-crystals, which is the factor presently limiting cost. Dislocations may play a significant role in defining the achievable size of high-resolution crystals. Scintillator detectors have some operational advantages when high-resolution spectroscopic detection is not required, namely, (i) they can be activated (doped) to detect different types of radiation (*e.g.*, gamma vs. neutron), (ii) they can have large volumes, and (iii) they can be inexpensive. In particular, glass scintillators are interesting compared to crystalline scintillators due to the potential cost advantage, as well as the ability to be easily formed into different shapes, fibers, or coatings, similar to plastic scintillators but with higher potential performance due to their higher density. Thus, glass scintillators can find use in a number of applications including portal monitors, *in situ* container monitors, tracking detectors, applications in extreme radiation environments, etc.

In addition, improved computational tools for materials design will result from this project, with broad applicability. In particular, advances in large-scale modeling of interfaces and dislocation electronic structure, leveraging world-leading high performance computing resources, will be useful for future "real" materials design efforts which need to account for structures in real devices. Advances in modeling the electronic structure of glass materials will contribute greatly to future rational design and optimization of glass scintillators, for the high-impact applications described above.

USERS

The direct users of the output of this project will be our experimental collaborators, who will fabricate improved materials and detectors (see the "Collaborators" section). The general community of material and detector producers (in industry, universities, and national laboratories) also would benefit.

The ultimate users of improved materials for high-performance radiation detectors include those agencies fielding such detectors for counter- and non-proliferation missions, including DOE, DOD, and DHS.

RESEARCHERS

Vincenzo Lordi is the principle investigator for the project, responsible for project management and direction, oversight, and application of the theoretical methods. He has 15 years experience in materials modeling, spanning from quantum-mechanics-based first-principles methods to

semi-empirical potential methods to meso-scale coarse-grained methods to continuum-level device modeling. His expertise ranges across density functional theory, quantum Monte Carlo, kinetic Monte Carlo, molecular dynamics, and TCAD device modeling. He also has extensive experience in experimental crystal growth; material characterization using optical, X-ray and electron spectroscopy as well as electron microscopy; and device fabrication. Much recent work has focused on studying the effects of defects in semiconductors on their electronic and optoelectronic properties, including more than 5 years as PI of NA22-funded projects studying materials for room-temperature radiation detectors. A characteristic of his work is the close coupling of theory with experiment. B.S.E in chemical engineering from Princeton, M.S. in electrical engineering from Stanford, Ph.D. in materials science & engineering for Stanford, Hertz Fellow, Lawrence Fellow. Led industrial R&D for a new product at KLA-Tencor Corp. before becoming a career physicist at LLNL. Over 35 publications or book chapters (cited 1300+ times; h-index of 13) and 5 patents.

Selected recent publications:

1. **V. Lordi**, "Point Defects in Cd(Zn)Te and TlBr: Theory," *Journal of Crystal Growth* **379**, 84 (2013). [Invited article for special issue]
2. C. Rocha-Leão and **V. Lordi**, "Ionic current and polarization effect in TlBr," *Physical Review B: Rapid Communications* **87**, 081202(R) (2013).
3. C. Rocha-Leão and **V. Lordi**, "Simultaneous control of ionic and electronic conductivity in materials: Thallium bromide case study," *Physical Review Letters* **108**, 246604 (2012).
4. C. Rocha-Leao and **V. Lordi**, "Ab initio guided optimization of GaTe for radiation detection applications," *Physical Review B* **84**, 165206 (2011).
5. **V. Lordi**, P. Erhart, and **D. Åberg**, "Charge carrier scattering by defects in semiconductors," *Physical Review B* **81**, 235204 (2010).
6. T.T.M. Vo, A.J. Williamson, **V. Lordi**, G. Galli, "Atomistic design of thermoelectric properties of silicon nanowires," *Nano Letters* **8**, 1111 (2008).
7. **V. Lordi**, H.B. Yuen, S.R. Bank, M.A. Wistey, S. Friedrich, and J.S. Harris, "Nearest neighbor distributions in GaInNAs(Sb) upon annealing," *Physical Review B* **71**, 125309 (2005).
8. **V. Lordi**, V. Gambin, S. Friedrich, T. Funk, T. Takizawa, K. Uno, and J.S. Harris, "Nearest-neighbor configuration in (GaIn)(NAs) probed by x-ray absorption spectroscopy," *Physical Review Letters* **90**, 145505 (2003). [Accepted without revision]

Nicole Adelstein is a postdoctoral fellow in the Quantum Simulations Group of the Condensed Matter and Materials Division of LLNL. She hold a Ph.D. in materials science from the University of California at Berkeley, where she studied electronic, ionic, and polaronic transport in rare-earth phosphates using first-principles methods. Her recent work at LLNL has included studying the electronic and magnetic properties of surface defects in quartz and silica, as well as the structure of glassy materials. She will work primarily on the glass scintillator aspect of this project, generating atomic structures and analyzing their electronic properties.

Selected recent publications:

1. **N. Adelstein**, J.L. DuBois, and **V. Lordi**, "Magnetic fluctuations from oxygen deficient centers on the SiO_2 surface," (in preparation).
2. **N. Adelstein**, J.B. Neaton, M. Asta, and L.C. De Jonghe, "First-principles studies of proton-Ba interactions in doped $LaPO_4$," *Journal of Materials Chemistry* **22**, 3758 (2012).
3. **N. Adelstein**, B.S. Mun, H.L. Ray, P.N. Ross, J.B. Neaton, and L.C. De Jonghe, "Electronic structure and properties of cerium orthophosphate: theory and experiment," *Physical Review B* **83**, 205104 (2011).

Donghwa Lee is a postdoctoral fellow in the Quantum Simulations Group of the Condensed Matter and Materials Division of LLNL. His experience has focused on using first-principles computational methods to study material behavior at various interfaces including crystal domain walls, organic-inorganic semiconductor interfaces, and water-oxide surfaces. He has applied diverse computational approaches, including density functional theory, quantum Monte Carlo, molecular dynamics, and kinetic Monte Carlo, to understand the physical and chemical activity at material interfaces for applications ranging from CO_2 sequestration to photocatalysis to solid-oxide fuel cells and superconducting qubits. For this project, he will focus on studying the chemical and electronic effects at the semiconductor–electrode interface of TlBr, leveraging his strong background in the chemistry of solid–solid interfaces.

Selected recent publications:

1. **D. Lee**, J.L. DuBois, and **V. Lordi**, "Microscopic Sources of Paramagnetic Noise on α-Al_2O_3 Substrates for Superconducting Qubits," *Physical Review Letters* (in revision).
2. **D. Lee**, H. Xu, V. Gopalan, V. Dierolf, and S. R. Phillpot, "Shape of Ferroelectric Domains in LiNbO3 and LiTaO3 from Defect/Domain-Wall Interactions," *Appl. Phys. Lett.* **98**, 092903 (2011).
3. **D. Lee**, H. Xu, V. Gopalan, V. Dierolf, and S. R. Phillpot, "Structure and Energetics of Domain Walls in LiNbO3," *Phys. Rev. B* **82**, 014104 (2010).
4. **D. Lee**, R. K. Behera, P. Wu, H. Xu, S. B. Sinnott, S. R. Phillpot, L.-Q. Chen and V. Gopalan, "Mixed Bloch-like and Néel-like Character to 180° Ferroelectric Walls in Lithium Niobate," *Physical Review B* **80**, 060102 (R) (2009).

Daniel Åberg is a staff member in the Condensed Matter and Materials Division of LLNL. He is an expert in first-principles materials modeling, including density functional theory and beyond-DFT methods such as hybrid functionals and the *GW* method. He has been a core member of the radiation detector materials modeling team at LLNL since beginning as a post-doc in 2006, and has focused on CdTe and CZT in recent years. His primary role will be to support the postdoc working on dislocations in CdTe. He also has experience in modeling the electronic structure of silica glass and leads a computational effort studying the physics of crystalline scintillators; he will play a consulting role on the glass scintillator task.

Selected recent publications:

1. **D. Åberg**, P. Erhart, and **V. Lordi**, "Contributions of point defects, chemical disorder, and thermal vibrations to electronic properties of $Cd_{1-x}Zn_xTe$ alloys," *Physical Review B* **88**, 045201 (2013).
2. B. Sadigh, P. Erhart, **D. Åberg**, A. Trave, E. Schwegler, and J. Bude, "First-Principles Calculations of the Urbach Tail in the Optical Absorption Spectra of Silica Glass," *Physical Review Letters* **106**, 027401 (2011).
3. P. Erhart, **D. Åberg**, B.W. Sturm, K.-J. Wu, and **V. Lordi**, "Theory-Guided Growth Of Aluminum Antimonide Single Crystals With Optimal Properties For Radiation Detection," *Applied Physics Letters* **97**, 142104 (2010).
4. P. Erhart, **D. Åberg**, and **V. Lordi**, "Extrinsic point defects in aluminum antimonide," *Physical Review B* **81**, 195216 (2010).
5. **D. Åberg**, P. Erhart, A.J. Williamson, and **V. Lordi**, "Intrinsic point defects in aluminum antimonide," *Phys. Rev. B* **77**, 165206 (2008).
6. M. Engholm, L. Norin and **D. Åberg**, "Strong UV absorption and visible luminescence in ytterbium-doped aluminosilicate glass under UV excitation," *Opt. Lett.* **32**, 3352 (2007).

Vasily Bulatov is a leading expert in dislocation theory and mesoscale materials modeling, and original co-author of the ParaDIS dislocation dynamics code. He will contribute expertise to the dislocation portion of the project, helping to generate models of dislocations and providing overall guidance in execution of that portion of the work. He has authored or co-authored numerous papers and books/book chapters on dislocation structure and dynamics. Currently staff scientist in the Condensed Matter & Materials Division at LLNL, former Teller Fellow, William and Mary Greve Foundation Fellow, and Fellow of the American Physical Society.

Selected recent publications:

1. **V. V. Bulatov** and W. Cai. *Computer Simulations of Dislocations*. (Oxford University Press, 2006).
2. **V. V. Bulatov**, W. Cai, J.P. Chang, J. Li, and S. Yip, "Dislocation core structure and mobility," in: *Dislocations in Solids*, volume 13, edited by F.R.N. Nabarro, (2003)
3. **V. V. Bulatov**, W. Cai, J. Li, J.P Chang, and S. Yip, "Periodic image effects in dislocation modelling," *Philosophical Magazine A* **83**, 539 (2002).
4. **V. V. Bulatov** and W. Cai, "Nodal effects in dislocation mobility," *Physical Review Letters* **89**, 115501 (2002).
5. W. Cai, **V. V. Bulatov**, J. Chang, J. Li, and S. Yip, "Anisotropic Elastic Interactions of a Periodic Dislocation Array," *Physical Review Letters* **86**, 5727 (2001).

PRIOR WORK

Through NA-22 support, our team has dedicated the past 6+ years to the development and application of predictive modeling methods to understand fundamental impediments to the

performance of materials for high-resolution, room-temperature gamma radiation detectors (LL07-FPSIM-PD05, LL10-Semi_Theory-PD05). The obtained knowledge was applied to design process strategies to improve materials performance, for a number of materials, including AlSb, GaTe, CdTe, CZT, and TlBr.[1,2,3,4,5,6,7,8,9,10] By working closely with experimental collaborators, we could both validate our predictions and also discover mitigation strategies to improve the materials after identifying the defects responsible for performance degradation. We developed a comprehensive computational toolkit for the rational evaluation of defect properties of materials and mitigation strategies. Some of the method innovations included development of a formalism to rapidly screen dopants and impurities for their impact on carrier mobility[11] and lifetime[6], application of systematically-converged hybrid functional calculations[9] as well as the quantum Monte Carlo method[12] to avoid band gap problems with standard density functional theory, and detailed evaluation of alloy effects[13]. Following we highlight several key results from our prior work.

We developed a predictive toolkit based on first-principles quantum mechanical simulations to assess the limits of "real" semiconductor materials for high-performance gamma radiation detectors. Parameter-free prediction of carrier mobilities, carrier lifetimes, mass transport rates, and dopant electronic properties, as well as the interdependence on defects/impurities, phonons, alloying, and nonstoichiometry, allowed the design of targeted purification processes, as well as compensation doping, annealing, and other mitigation strategies for the target materials.

Recent work on TlBr focused on determining whether doping could be used to reduce ionic mobility and mitigate the "polarization" effect.[6,7] We were successful in inventing a co-doping strategy that limits ionic mobility without adversely affecting the carrier transport properties (mobility-lifetime product), which led to a patent application in addition to publications. We delivered our results to our experimental collaborators at RMD, who are incorporating our predicted optimal co-dopant pairs (Pb+Se or Pb+S) into their crystal growth processes. After achieving the goal of understanding dopant effects on ionic mobility in TlBr, we continued to explore other origins of the polarization phenomenon by studying the effects of contact metals in conjunction with our experimental collaborators at LLNL and RMD. We used our predictive modeling to screen more than a dozen candidate contact metals for detrimental effects associated with in-diffusion from either anode or cathode electrodes.[14] Our calculations were validated against measured device stability data for Ni, Au, Ag, and Cu contacts, and also for C and O impurities. We delivered to RMD the predicted best-choice contact metals to avoid carrier lifetime degradation from electrode in-diffusion: Ni or Pt for the anode; Cr, Ti, Mo (or possibly Bi) for the cathode. (In both cases, we ranked our suggestions by the calculated solubilities in TlBr.) Device stability data using the new contacts is forthcoming. Through our experimental collaborators at LLNL, we have already validated that Ni-Pt and Ni-Bi contact pairs improve device stability, as predicted.

For CdTe/CZT, we applied advanced theoretical techniques of unprecedented accuracy based on hybrid functional density functional theory to quantitatively analyze a range of intrinsic and extrinsic defects,[9] and, by comparing to experimental data from our collaboration with Ralph James' group at BNL, to identify the microscopic origin of important deep levels observed in spectroscopy experiments. Some important results include showing that a single Cd vacancy does not introduce deep levels into the material as had been previously believed, but that instead a Cd vacancy-related complex is the most likely origin of intrinsic deep acceptors in the material. Most likely, this complex is between a Cd vacancy and a Te antisite defect, for which we found

characteristic vibrational modes that would enable identification of this deep native acceptor experimentally. We also showed that Cd di-vacancies are not stable. Furthermore, we found that a specific type of Te interstitial, namely the split interstitial comprised of two Te atoms sharing a single Te site and oriented along a <110> crystal direction, is a low energy defect with high mobility in the crystal. Cd vacancies are the most prevalent defect and introduce shallow acceptors, while Cd interstitials are compensating donors (particularly at Cd-rich conditions, which is not typical of detector material). Furthermore, we studied O, Cl, In, Pb, and Bi impurities, for which DLTS data is available from BNL. Our results help to interpret deep level spectroscopy data and to understand how carrier lifetimes may be optimized.

Regarding Te secondary phases in CdTe/CZT, we used a combination of quantum mechanical calculations and semi-empirical kinetic modeling to discover a mechanism for Te clustering/ precipitation.[10] The important role of fast-diffusing Te split interstitials was identified for the first time, as well as the significance of interactions with Cd vacancies and Te antisites, to generate Te-rich regions in the crystal. This work enables both an understanding of the electronic structure of small Te-rich regions in the material, and also the design of annealing processes to manipulate the precipitates.

To understand the detailed effects of Zn alloying in CZT at different Zn concentrations, we evaluated explicitly the role of Zn disorder on the behavior of defects impacting charge transport.[13] The alloy effects were compared to the effects of point defects in a perfect lattice and to the effects of phonons, to evaluate the dominant carrier scattering mechanism as a function of temperature. Above 100 K phonons were found to dominate carrier scattering and mobility, but at lower temperatures alloy effects dominate.

We recently have begun a limited study on the atomic structure and electronic properties of single straight dislocations (edge and screw) in CdTe. By using a first-principles description of the forces on the inner core atoms and using special boundary conditions to accurately capture long-range strain effects, the electronic states associated with the dislocation core could be determined for a select set of ideal dislocations.[15] Modestly large-scale calculations involving 600–800 “quantum” atoms were required for these studies, embedded within 18,000-atom classical models of the long-range strain.

Earlier work focused on AlSb and GaTe materials. For AlSb, our exhaustive analysis of all native defects and nearly a dozen impurities/dopants led to a process strategy that improved both the mobility-lifetime product and the resistivity of the material by an order of magnitude, leading to high quality α-spectroscopic material.[3] The theory-led process design involved the use of H_2 in the Czochralski growth chamber to reduce detrimental O impurities and the addition of Te dopants to compensate background C impurities without impacting carrier mobilities significantly. We also discovered the possibility of a novel carrier compensation strategy based on ambipolar Sn dopants and programmed annealing.[2] The work resulted in a patent application in addition to several publications. Our developed methods for high-throughput computational screening of the effects of different defects on carrier mobility and lifetime were instrumental in those achievements. The close collaboration with our experimental partners was also crucial. Using a similar approach, for GaTe, we showed that Ga-rich growth combined with Ge ambipolar doping could maximize resistivity while not sacrificing mobility.[5]

In addition to the work on radiation detector materials outlined above, several team members, including the PI, have experience with or are actively working on using simulation techniques to study the electronic properties of various glass materials. A current LDRD project at LLNL (PI: Schaffers) is focused on developing a glass material for the National Ignition Facility (NIF) to filter stray infrared light without attenuating the main ultraviolet beam, a needed critical optic. The PI and co-workers are using simulations to understand how metal dopants in glass interact with neighboring ligands to modify the absorption spectrum, to enable optimization of the composition and/or melt process to meet the filter requirements. Additionally, recent work by a team member studying optical absorption in the Urbach tail of silica glass using first-principles calculations revealed that a Poisson process dominates absorption by the tail states, leading to large fluctuations that reduce thermal runaway.[16]

Finally, the PI has 15 years experience with materials modeling in general, as well as experience in experimental crystal growth, materials characterization, and semiconductor device fabrication. The "Researchers" section above further highlights the relevant backgrounds of each team member for the proposed work of this project.

COLLABORATORS

We will continue to collaborate closely with Radiation Monitoring Devices, Inc. (RMD) on the TlBr portion of the project. RMD is a leader in producing high-quality TlBr crystals for radiation detectors. They will provide experimental support for our work, both for validation and as customers of our results on optimal material/device fabrication. We will also continue to collaborate with an experimental team at LLNL (PI: Conway), who are studying surface/interface effects on the device stability of TlBr. We already have established relationships with both the RMD and LLNL teams from our previous Lifecycle. They are both funded through DHS/DNDO, which is committed to supporting the development of TlBr.

Regarding the glass scintillator host material portion of the proposed work, the initial phase will be computational (the generation and analysis of structures) and rely on existing literature data for validation. Once the baseline material models are established, exploration of process and compositional variations will proceed in the 2nd and 3rd years. At that latter stage, collaboration with experimental groups to test predictions will be pursued. We will target collaborations both with national labs, for example L. Boatner, *et al.* at Oak Ridge National Lab, and with LLNL and industrial glass producers with which we already have relationships for our work with the National Ignition Facility at LLNL.

We have maintained a working relationship with Brookhaven National Laboratory (R. James, *et al.*) for experimental work on CZT from the prior Lifecycle. We will maintain this relationship for this project, with the main technical contribution being electron microscopy of dislocation patterns in the material. We will also establish a cooperative relationship with Sandia National Laboratory (F.P. Doty, *et al.*). The team at Sandia has developed and validated an empirical bond-order potential for CdTe that will be useful to generate starting configurations of large dislocation network structures.[17] In addition, the Sandia team has proposed complementary work associated with dislocations in CZT, related to the mechanical properties during growth and controlling grown-in dislocation densities. Our work focuses on understanding the fundamental electronic properties of dislocation networks in the material, with and without decoration.

Together, our projects complement each other and address a comprehensive set of questions related to the effects and properties of dislocations in CZT affecting crystal quality for high-performance room-temperature radiation detectors.

WORK FOR OTHERS

None.

PROPOSED WORK AND SCIENTIFIC BASIS

We propose to extend our modeling efforts by leveraging semi-empirical methods in conjunction with first-principles methods to perform multi-scale, multi-resolution simulations of materials for high-performance gamma radiation detectors. The focus is split between high-potential-impact semiconductors and an emerging class of scintillators based on glass. This focus balances high-value shorter-term impact with higher-risk/high-payoff longer-term research, while leveraging the unique capabilities and resources of this team. The three aspects (not equally weighted) of the proposed work are: (i) optimization of materials used at the electrical contact interfaces of TlBr detectors to produce temporally stable detectors at room temperature; (ii) elucidation of the electronic structure of glass host materials for scintillators, to enable design of hosts for high-performance detectors; and (iii) determination of the electronic properties (carrier trapping) of dislocation networks in CdTe/CZT.

Here we outline the scientific basis and general proposed work we will use to address these three problems. Details of specific tasks and the associated project timelines are found in the "Statement of Work Task List." Not all tasks are concurrent, and emphasis will vary through the lifecycle.

A. TlBr Contacts and Interface Effects

TlBr remains a top candidate for high-resolution (<1% at 662 keV) room-temperature gamma spectroscopy, as it possesses essentially all of the required material properties (moderate band gap, high Z, long drift length, and high room-temperature resistivity).[18] The material is one of only a few candidate semiconductors poised for a major breakthrough in the next few years, with high-performance already demonstrated.[19] However, temporal degradation of performance from the so-called "polarization" effect remains a hurdle to large-scale commercialization, despite some recent advances.[20,21,22,23]

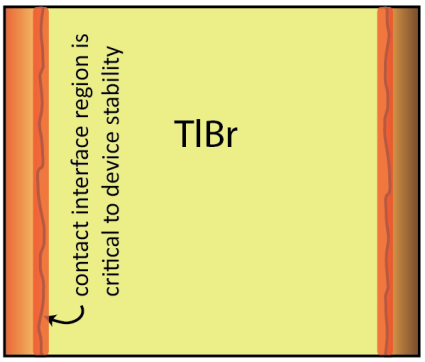

Figure 1. Interface effects at the electrical contacts of TlBr detectors play a major role in detector stability.

A plausible path forward to stable, room-temperature operation of TlBr is in sight. We have already studied the role (co-)dopants can play on reducing ionic mobility (see "Prior Work" section).[6] Based on our prior theoretical work and the experimental work of our collaborators and others[23], it appears that contact and interface effects are the current dominant contributors to device degradation ("polarization").

We propose to extend our previous studies of TlBr to address the crucial effects of chemistry and electrochemistry at the TlBr/metal interfaces. We will also study the properties of engineered contact stacks, which may include a heterojunction between the TlBr and the contact metal. Such a heterojunction material may either be deposited or may be formed chemically during fabrication by exposing TlBr to various wet chemicals, for example HCl etching to form $TlBr_xCl_{1-x}$, as suggested by our LLNL collaborators. We wish to determine the temporal evolution of the chemical and electronic structure of the contact interface(s) to make connections to device stability. For example, electrochemical reactions driven by Fermi-level shifts at the interface, associated with the work function of a contact metal, can cause detrimental long-term material transformations.

Density functional theory will allow the calculation of reaction thermodynamics to determine stable phases at the interface. We will then use first-principles methods based on DFT and beyond to determine the electronic states at the interfaces, based on atomic models constructed of those interfaces. Since the Fermi level at the interface is a critical parameter governing electrochemical reactions, a determination of Fermi-level pinning from interface electronic states is crucial and will also result from the calculations. These parameters, along with the previously determined bulk electronic and ionic transport properties, allow connection to device electrical performance and stability.

We will continue to collaborate closely with the experimental teams at LLNL and RMD to make connections with and advance the state-of-the-art of real devices.

B. Glass Scintillators

Glass (non-crystalline) materials can be very favorable for radiation detection due to the potential for low-cost, large-volume fabrication of easily formable cast shapes, fibers, or spun coatings with high density and intrinsic radiation tolerance, as well as thermal, mechanical, and chemical stability.[24] The composition of the glass can be tailored to be sensitive to the absorption of either gamma rays or neutrons, and dopants (typically Ce^{3+}) are used to impart scintillating property. However, the light yield and energy resolution demonstrated to-date for glass scintillators have been far inferior to those for single-crystal scintillators. Current performance is insufficient for applications in detecting SNM movement, and today utility is only found for applications in extreme radiation environments.[24]

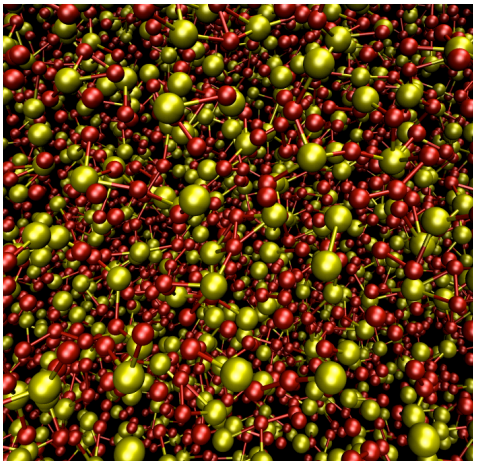

Figure 2. Modeling reveals the detailed correlation between atomic and electronic structure in glass. Shown is a model of silica glass generated with molecular dynamics.

The potential pay-off of developing high-performance glass scintillators for gamma or neutron detectors is very high. However, the severe underperformance of current state-of-the-art materials indicates that better fundamental understanding of the physical mechanisms of scintillation in glass is needed. Past experimental efforts have revealed a connection to the broad distribution of local chemical environments found in a glass, which can lead to a broad distribution of activator energy levels and possible variations in activator oxidation state as well, both of which will degrade the intensity of emitted light in the measured wavelength band. Also,

poor carrier transport in typical glass materials often limits the average distance that radiation-induced carriers can travel to reach an activator, requiring higher activator doping levels compared to crystalline materials. Thus, rational design of improved glass hosts for bright scintillators requires gaining knowledge of the correlation of glass chemistry with atomic structure and charge transport, as well as the effects on activator dopant incorporation/solubility. Fundamental limits on charge transport need to be understood, so that glass compositions may be manipulated to systematically improve performance.

We will use simulations to gain fundamental insight into the correlations between composition, structure, and performance of scintillating glasses. The distribution of local structure for different glasses and the dependence on composition will be determined and correlated with the electronic structure of the glass matrix. A combination of semi-empirical atomistic simulations and first-principles based simulations will be used to generate structural models and analyze the electronic properties of candidate glass materials. A major activity will be to determine the range of heterogeneity in a given glass and how best to generate representative structures. A standard approach to creating an atomistic model of a glass is to create a melt computationally, then cool the system to simulate the glass solidification process. However, since accessible simulation times are limited compared to actual relaxation rates in a cooling glass, a critical step in the computational process involves "annealing" or "repairing" excess dangling bonds that result from the quench step. Various approaches will be explored for this critical step, including bond-switching,[25] the activation-relaxation technique,[26] and Monte Carlo methods. Ultimately, the resulting structures will be verified by comparing computed structure factors to measured structure data from the literature.

Our proposed approach for this task is to use a systematic progression of complexity, beginning with better-known systems such as silicates before progressing to a broader exploration of compositional effects. The goal is to gain fundamental knowledge characterizing the structural and electronic features of different glasses so that material design and optimization may be possible in the future. In fact, our very initial work will be on amorphous silica, which provides a useful test case with extensive data available on its structure and electronic properties for validation.[27]

Comparison of the electronic structure of known poor- and better-performing glasses will help reveal favorable structural features. With a baseline knowledge established, novel glass families can be explored, for example germinates, non-fluoride halides, borates, and tungstates, to maximize charge transport in the host. Much past work has focused on silicate glasses[28,29] (indeed Ce-activated Li-silicate glass is available commercially), with some work on phosphates[30] and fluorides[31], but a broader range of glass families warrants exploration. Amorphous halides (chlorides, bromides, iodides) may be particularly interesting, due to their relationship to high-performing crystalline scintillators. The stretch goal is to produce a glass that approaches its theoretical light yield and energy resolution, at least comparable to crystalline scintillators such as NaI or $LaBr_3$; the proposed work will make inroads to enable that possibility. We expect to explore at least 3 different glass systems over the course of the project.

C. Dislocations in CZT

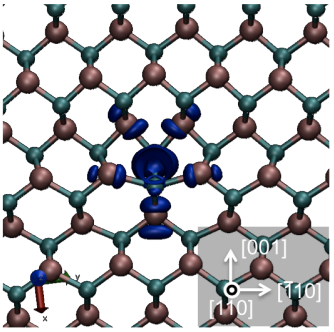

$Cd_{1-x}Zn_xTe$ (CZT) is the most mature and highest performing room-temperature semiconductor gamma radiation detection material.[32] Despite recent improvements, problems in crystal growth persist that make the material cost prohibitive for large volume detectors and for ubiquitous applications. A major area needing further research is the role of extended dislocation structures, particularly dislocation "walls"[33], in limiting electrical performance (mediating carrier capture) and the means to eliminate them. Related is the question of the role of Te-rich regions (precipitates or inclusions) and other impurities that often are observed to "decorate" dislocations.[33,34] Since it is nearly impossible to separate these effects experimentally, we aim to determine first the fundamental electronic properties (carrier capture propensity) of dislocations in CdTe (we have already shown that we can reliably use CdTe as a proxy for CZT) and then to resolve the question of what plays the primary role in carrier capture: the dislocations or the impurities/precipitates. This issue may be the final aspect of attaining the full potential of CZT detectors. The expected outcome would be improved detector electrical performance by reducing the tail/sideband of the photopeak, improving resolution and signal intensity.

We propose to tackle this task by extending our current work on the atomic and electronic structure of single dislocations in CdTe. An approach of systematic progression of complexity will be taken, based on the team's prior experience with the properties of extended dislocation structures. First, we must sample a wide variety of dislocation structures, including partial dislocations and various possible core structures, to determine the variety of electronic properties of dislocations that occur in the material. Secondly, we will extend our simulations of straight dislocations to kinked dislocation lines, which we can treat directly with density functional theory for system sizes of thousands of atoms. The electronic properties of a kink will reveal much about the properties of extended dislocation networks,[35] giving a more accurate representation of the structure of real crystals, which often have many sub-grains. These simulations will comprise a baseline understanding of the electronic (carrier trapping) effects of dislocations in Cd(Zn)Te, which is presently lacking. In fact, detailed understanding of the electronic properties of dislocations in semiconductors in general is presently immature, and this work will be pioneering by leveraging high-performance computing and in-house highly-scalable DFT codes to treat systems with large numbers of atoms (several thousand+).

Ultimately, we aim to coordinate our simulations with experimental thermal annealing studies coupled with characterization of dislocation densities and the resulting transport properties. By quantitatively comparing our predictions to measurements, we can deduce whether the dislocation networks alone can explain the magnitude of transport degradation or if their "decoration" is responsible, a determination that would be extremely difficult or impossible to make solely experimentally. Much prior work has already been done on the role of Te precipitates in carrier capture, both by others and ourselves, using continuum-level[36] and atomic-level simulations[10] as well as experiments.[32] Our own prior work has focused on the atomic and electronic structure of microscopic precipitates.[8,10] This existing knowledge can be input into continuum models of dislocation networks using an existing modeling framework[36] to assess what degree of association of Te precipitates with dislocations is required to match observed carrier transport properties.

TECHNICAL ISSUES

The technical approaches we will employ for this project are outlined in the "Proposed Work and Scientific Basis" section above. Risks associated with technical hurdles vary with the aspect of the project, which balances shorter-term lower-risk deliverables with higher-risk longer-term goals. Here we outline the technical risk profile of each aspect of the proposed work and describe our mitigation plans.

The TlBr portion of the proposed work is considered the lowest risk. We have extensive experience modeling bulk TlBr from our previous Lifecycle and considerable team experience modeling interfaces generally. In addition, our previous computational results as well as experimental results of our collaborators strongly suggest that the remaining obstacle to producing temporally stable TlBr detectors with high sensitivity and energy resolution is related to interface effects, so we believe our focus in this project has a high likelihood of producing high impact. A technical hurdle is the potential computational complexity of creating realistic interface models, which may be characterized by thick interface regions. This problem is mitigated by the fact that simple models often describe the behavior of the interface accurately, at least in the short-range. Empirical methods will be used, combined with highly parallel exploration of structural phase space leveraging our massively parallel supercomputers, to generate more complex structures, from which local motifs can be extracted and explored at the electronic structure level. This approach is feasible since chemistry, carrier trapping, and mass transport at solid–solid interfaces are usually local effects on the scale of DFT system sizes.

For the glass portion of the project, the major technical challenge is the construction of realistic atomistic models for a glass, particularly with complex compositions. Since the glass is amorphous, care must be taken to generate models that do not include non-physical dangling bonds, for example. We must also take care to reproduce local structure accurately, which we can characterize with radial distribution functions (structure factors) and compare to experimental characterization. A standard method to generate a glass model is to perform a melt simulation, followed by re-solidification into the amorphous state. By following this procedure with a careful annealing procedure, we can produce well-behaved glass models. We will leverage our prior experience to overcome these technical challenges, with the methods mentioned in the "Proposed Work and Scientific Basis" section, as well as our access to large supercomputing resources that enable suitable exploration of the large configuration space. In addition, our work will feed-back to experiments by gaining insight into the range of local structures that can result from differences in synthesis conditions, which we can simulate, for example, by varying the cooling rate in the re-solidification simulations. Thus, part of the technical hurdle becomes a technical advantage by revealing the sensitivities.

For the dislocation work, the major challenge is to make connection to realistic dislocation structures in CZT crystals, so that we may determine their electronic structure. From our experience with the diamond cubic/zinc-blende crystal structure, we know the common structures that form, such as dislocation walls/low-angle grain boundaries and twist boundaries, which we can correlate with observations. We can also leverage experimental observations from the literature and our collaborators to understand the general configuration of the networks. Then, the major task is to generate atomistic models sufficiently large to capture enough of the network structure, but also small enough to tractably treat with electronic structure methods. Our previous work suggests that small models can go a long way to describing the electronic

properties of the dislocation core, particularly for a covalently bonded material. In fact, a modestly-sized model of a kinked dislocation line can reveal much about the electronic structure of more complex dislocation structures. For the most complex models intended to be simulated toward the end of the project Lifecycle, we may require on the order of several thousand atoms. To treat those largest systems, we will leverage empirical potentials to generate close starting structures and our in-house linear-scaling DFT codes (MGmol, and the in-development DG-DFT code) to evaluate the electronic states. Our specialized, in-house, highly-scalable DFT codes enable electronic structure calculations to be performed on systems of the order of 10,000 atoms by scaling to tens of thousands of processor cores or more on our massively-parallel supercomputers.

Leverage of LLNL Institutional Resources

This research project is well positioned to leverage the extensive supercomputing resources available at LLNL, at no direct cost to NA-22, including the 431 TFLOP/s (20,736 CPUs) Cab cluster, the 44 TFLOP/s (3888 CPUs) Ansel cluster, the 5 PetaFLOP/s (393,216 CPUs) Vulcan cluster, and the 261 TFLOP/s (23,328 CPUs) Sierra cluster, among other computing resources. This computing capability is leveraged in combination with a number of unique software tools, including those developed by the PI and team during prior NA-22 funded work and also prior LDRD, DARPA, and DOE Office of Science projects. A notable capability is a real-space, $O(N)$, linear scaling density functional theory code (MGmol) developed by a collaborator at LLNL which enables the calculation of electronic structure of systems with tens of thousands of atoms using tens of thousands of processor cores.

The powerful combination of state-of-the-art algorithms and world-leading supercomputer facilities at LLNL has enabled the authors of this proposal to perform some of the largest, most accurate, and most complete electronic structure simulations of semiconductor materials and their defects to date. The multi-scale, multi-physics aspects of this proposed project will enable the team to further advance the state-of-the-art. A unique aspect of much of the team's prior work, enabled by the access to massively-parallel supercomputing resources, has been the special attention paid to understanding and controlling the sources of error in the calculations to quantify the accuracy.

REFERENCES

[1] D. Åberg, P. Erhart, A.J. Williamson, and V. Lordi, "Intrinsic point defects in aluminum antimonide," *Phys. Rev. B* **77**, 165206 (2008).

[2] P. Erhart, D. Åberg, and V. Lordi, "Extrinsic point defects in aluminum antimonide," *Physical Review B* **81**, 195216 (2010).

[3] P. Erhart, D. Åberg, B.W. Sturm, K.-J. Wu, and V. Lordi, "Theory-Guided Growth Of Aluminum Antimonide Single Crystals With Optimal Properties For Radiation Detection," Applied Physics Letters, 97, 142104 (2010).

[4] V. Lordi, D. Åberg, P. Erhart, K.J. Wu, "First principles calculation of point defects and mobility degradation in bulk AlSb for radiation detection application," *Proc. SPIE* **6706**, 67060O (2007).

[5] C. Rocha-Leao and V. Lordi, "Ab initio guided optimization of GaTe for radiation detection applications," *Physical Review B* **84**, 165206 (2011).

[6] C. Rocha-Leão and V. Lordi, "Simultaneous control of ionic and electronic conductivity in materials: Thallium bromide case study," *Physical Review Letters* **108**, 246604 (2012).

[7] C. Rocha-Leão and V. Lordi, "Ionic current and polarization effect in TlBr," *Physical Review B: Rapid Communications* **87**, 081202(R) (2013).

[8] V. Lordi, "Point Defects in Cd(Zn)Te and TlBr: Theory," *J. of Crystal Growth* **379**, 84 (2013). (Special edition in tribute to Prof. Michael Schieber)

[9] P. Erhart, D. Åberg, and V. Lordi, "Intrinsic point defects in CdTe studied using hybrid density functional theory calculations," Materials Research Society Spring Meeting, YY3.3, San Francisco, April 27 (2011); P. Erhart, D. Åberg, and V. Lordi, "Intrinsic point defects in cadmium telluride studied using hybrid density-functional theory calculations," *Physical Review B*, in preparation.

[10] V. Lordi, "Mechanisms and kinetics of tellurium clustering in CdTe," American Physical Society March Meeting, L24.3, Boston, Feb 28 (2012); V. Lordi, "Mechanisms and kinetics of tellurium clustering in CdTe," TMS Annual Meeting, Orlando, March 14 (2012).

[11] V. Lordi, P. Erhart, and D. Åberg, "Charge carrier scattering by defects in semiconductors," *Physical Review B* **81**, 235204 (2010).

[12] J. DuBois, D. Åberg, R.Q. Hood, and V. Lordi, "Diffusion Monte Carlo calculations of charged defects in semiconductors," Gordon Research Conference on Defects in Semiconductors, Colby-Sawyer College, New London, NH, August 8-13 (2010).

[13] D. Åberg, P. Erhart, and V. Lordi, "Contributions of point defects, chemical disorder, and thermal vibrations to electronic properties of $Cd_{1-x}Zn_xTe$ alloys," *Physical Review B* **88**, 045201 (2013).

[14] C. Rocha-Leão and V. Lordi, "Effects of contact metal impurities in TlBr radiation detectors," in preparation.

[15] M. Skarlinski, E. Cho, D. Åberg, and V. Lordi, "Atomic and electronic structure of dislocations in CdTe," SPIE Optics+Photonics, 8852-8, San Diego, Aug 26 (2013).

[16] B. Sadigh, P. Erhart, D. Åberg, A. Trave, E. Schwegler, and J. Bude, "First-Principles Calculations of the Urbach Tail in the Optical Absorption Spectra of Silica Glass," *Physical Review Letters* **106**, 027401 (2011).

[17] D.K. Ward, X.W. Zhou, B.M. Wong, F.P. Doty, and J.A. Zimmerman, "Analytical bond-order potential for the cadmium telluride binary system," *Physical Review B* **85**, 115206 (2012).

[18] K. Hitomi, Y. Kikuchi, T. Shoji, and K. Ishii, *IEEE Trans. Nucl. Sci.* **56**, 1859 (2009).

[19] K. Hitomi, M. Matsumoto, O. Muroi, T. Shoji, and Y. Hiratate, *IEEE Trans. Nucl. Sci.* **49**, 2526 (2002).

[20] A.V. Churilov, G. Ciampi, H. Kim, L.J. Cirignano, W.M. Higgins, F. Olschner, and K.S. Shah, *IEEE Trans. Nucl. Sci.* **56**, 1875 (2009)

[21] A.M. Conway, L.F. Voss, A.J. Nelson, P.R. Beck, R.T. Graff, R.J. Nikolic, S.A. Payne, H. Kim, L.J. Cirignano, and K. Shah, "Long-term room temperature stability of TlBr gamma detectors," *Proc. SPIE* **8142**, 81420J (2011).

[22] I. B. Oliveira, F. E. Costa, P. K. Kiyohara, and M. M. Hamada, *IEEE Trans. Nucl. Sci.* **52**, 2058 (2005).

[23] K. Hitomi, T. Shoji, and Y. Nlizeki, *Nucl. Instrum. Methods Phys. Res., Sec. A* **585**, 102 (2008).

[24] see, e.g., C.W.E. van Eijk, "Inorganic-scintillator development," *Nuclear Instruments and Methods in Physics Research A* **460**, 1 (2001).

[25] F. Wooten, K. Winer, and D. Weaire, "Computer Generation of Structural Models of Amorphous Si and Ge," *Phys. Rev. Lett.* **54**, 1392 (1985).

[26] G.T. Barkema and N. Mousseau, "Event-Based Relaxation of Continuous Disordered Systems," *Phys. Rev. Lett*. **77**, 4358 (1996).

[27] J. Singh and Koichi, S., eds, *Advances in Amorphous Semiconductors (Advanced in Condensed Matter Science)*, (CRC Press, 2003).

[28] R. Spowart, "Measurement of the Gamma Sensitivity of Granular and Glass Neutron Scintillators and Films," *Nucl. Instr. Meth*., **82**, 1 (1970).

[29] M.J. Weber, M. Bliss, R.A. Craig, and D.S. Sunberg, "Scintillators and Applications: Cerium-Doped Materials," *Radiation Effects and Defects in Solids* **134**, 23 (1995).

[30] J. Neal, L. Boatner, D. Wisniewski, and J. Ramey, "New rare-earth activated phosphate glass scintillators," *Proceedings of the SPIE* **6706**, 670618 (2007).

[31] T. Murata, S. Fujino, H. Yoshida, Y. Arikawa, T. Nakazato, T. Shimizu, N. Sarukura, M. Nakai, T. Norimatsu, H. Azechi, K. Kamada, Y. Usuki, T. Suyama, A. Yoshikawa, N. Sato, and H. Kan, "Custom-Designed Fast-Response Praseodymium-Doped Lithium 6 Fluoro-Oxide Glass Scintillator With Enhanced Cross-Section for Scattered Neutron Originated From Inertial Confinement Fusion," *IEEE Trans. on Nuclear Sci.* **57**, 1426 (2010).

[32] T.E. Schlesinger, J.E. Toney, H. Yoon, E.Y. Lee, B.A. Brunett, L. Franks, and R.B. James, "Cadmium zinc telluride and its use as a nuclear radiation detector material," *Materials Science and Engineering* **32**, 103 (2001).

[33] J.A. Zimmerman, D.K. Ward, F.P. Doty, B.M. Wong, X.W. Zhou, "Towards improved CZT crystals," Symposium on Radiation Measurements and Applications, Ann Arbor, MI, May 24-28, (2010).

[34] A. Hossain, A.E. Bolotnikov, G.S. Camarda, Y. Cui, G. Yang, and R.B. James, "Defects in cadmium zinc telluride crystals revealed by etch-pit distributions," *Journal of Crystal Growth* **310**, 4493 (2008).

[35] V.V. Bulatov and W. Cai. *Computer Simulations of Dislocations*. (Oxford University Press, 2006).

[36] A.E. Bolotnikov, G.S. Camarda, G.A. Carini, Y. Cui, L. Li, R.B. James, "Cumulative effects of Te precipitates in CdZnTe radiation detectors," *Nuclear Instruments and Methods in Physics Research A* **571**, 687 (2007).

----------End of Project Narrative---------

STATEMENT OF WORK TASK LISTING

STATEMENT OF WORK TASK LISTING FOR FY 2014:

FY 2014 TASKS:

1. Build atomistic chemical models of TlBr–metal interfaces
2. Generate atomistic models for two glass hosts
3. Build and determine electronic structure of various straight dislocations in CdTe

Task 1: **Build atomistic chemical models of TlBr–metal interfaces**
This task involves construction of atomic-scale interface models for candidate metal contacts with TlBr. Work on this task will begin in the second half of FY2014 and continue in FY2015, when analysis of the thermodynamics of phases that may form at the interface will further take place.

FY 2014 TECHNICAL MILESTONES

09/30/2014 — Complete construction of atomistic interface model for 1 relevant metal

Task 2: **Generate atomistic models for two glass hosts**
This task will use empirical and/or *ab initio* potentials to generate glass models by the computational melt–re-solidification process and appropriate post-solidification annealing.

FY 2014 TECHNICAL DELIVERABLES

09/30/2014 — Deliver report contrasting atomic structure motifs of two glass models and validation data to NA-22

FY 2014 TECHNICAL MILESTONES

11/30/2014 — Validate structure and electronic density of states of amorphous silica test-case
02/15/2014 — Construction of first complete glass model
03/30/2014 — Analysis of structure factor of model and comparison to experimental data from literature
08/30/2014 — Completion of two comparative glass models

Task 3: **Build and determine electronic structure of various straight dislocations in CdTe**
This task will generate a database of the electronic structure of a broad class of straight dislocations in CdTe, as a baseline to study more complicated dislocation networks.

FY 2014 Technical Deliverables

06/30/2014 — Submit manuscript on atomic and electronic structure of straight dislocations in CdTe to a peer-reviewed journal

FY 2014 Technical Milestones

01/31/2014 — Obtain electronic gap states of a single straight edge dislocation, as a function of distance from the core
03/30/2014 — Use empirical potentials combined with density functional theory to generate structures and determine the electronic states of a set of at least 6 dislocations in CdTe

Statement Of Work Task Listing For FY 2015:

FY 2015 Tasks:

1. Build atomistic chemical models of TlBr–metal interfaces (cont.)
4. Study heterostructure effects at TlBr–contact interface
5. Compare electronic structure motifs in different glass hosts
6. Build and determine electronic structure of kinked screw dislocation in CdTe

Task 1: **Build atomistic chemical models of TlBr–metal interfaces (cont.)**
This task continues Task 1 from FY2014 on construction of atomic-scale interface models for candidate metal contacts with TlBr. The interface thermochemistry will be analyzed to determine stable interphases which may form in operation, or may serve as heterostructure materials (subject of Task 4).

FY 2015 Technical Deliverables

09/30/2015 — Deliver report on chemical thermodynamics of TlBr–metal interfaces (at least 2 relevant metals) to NA-22

FY 2015 Technical Milestones

02/28/2015 — Complete construction of atomistic interface model for at least 2 relevant metals
04/30/2015 — Analysis of interface chemical thermodynamics, in terms of stable interface phases

Task 4: **Study heterostructure effects at TlBr–contact interface**
This task expands the complexity of the "real" interface model to include intermediate chemical layers and also involves the incorporation of electrochemical potential into the simulations

FY 2015 Technical Deliverables

09/30/2015 — Deliver report on heterostructure effects on device stability of TlBr detectors to NA-22

FY 2015 Technical Milestones

04/15/2015 — Construct interface models with heterostructure material between TlBr and metal
07/15/2015 — Determine electronic states and Fermi-level pinning of interfaces

Task 5: **Compare electronic structure motifs in different glass hosts**
This task involves analysis of the electronic states in the glass models generated in FY2014 and correlation with structural features (local order) present in each glass. The nature of the electronic states affect electronic transport and thus the ability to transfer energy to an activator atom, which affects scintillation efficiency.

FY 2015 Technical Deliverables

09/30/2015 — Submit manuscript on electronic structure of two glass hosts to peer-reviewed journal

Task 6: **Build and determine electronic structure of kinked screw dislocation in CdTe**
This task will use a large-scale first-principles model of a single kinked dislocation to study the electronic states.

FY 2015 Technical Deliverables

09/30/2015 — Submit manuscript on atomic and electronic structure of a kinked dislocation in CdTe to a peer-reviewed journal

FY 2015 Technical Milestones

01/30/2015 — Use empirical bond-order potential to generate initial structure of a kinked screw dislocation
03/30/2015 — Relax structure of kinked screw dislocation with density functional theory
07/15/2015 — Evaluate electronic density of states for kinked screw dislocation

Statement Of Work Task Listing For FY 2016:

FY 2016 Tasks:

7. Explore optimal layering for stable interfaces at TlBr–contact junctions
8. Analyze chemical and process dependence of electronic transport characteristics of glass hosts

9. Evaluate carrier trapping contributions from dislocations and "decoration" (impurities, precipitates)

Task 7: **Explore optimal layering for stable interfaces at TlBr–contact junctions**
As a continuation of Tasks 1 and 4, this task will search for optimal contact material(s) with chemical stability over time that will impart temporal stability to the TlBr detector device.

FY 2016 TECHNICAL DELIVERABLES

05/30/2016 — Deliver candidates for optimal TlBr contact structure/process to RMD and LLNL collaborators
09/30/2016 — Submit manuscript on improved contact design for TlBr detectors to peer-reviewed journal

FY 2016 TECHNICAL MILESTONES

03/30/2015 — Evaluate electrochemical potentials at interfaces from metal work functions

Task 8: **Analyze chemical dependence of electronic transport characteristics of glass hosts**
Building on the previous two years' results on the correlation between atomic structure and electronic states of specific glasses, this task will entail calculation of the electronic transport properties of the different glass hosts as well as expand on the correlation between processing/composition and electronic properties. These discoveries will lead to knowledge on how the chemistry, process, and/or composition of the glass host may be manipulated to create a glass with optimal carrier transport so that a large fraction of ionized carriers reach activator atoms, producing a bright scintillator.

FY 2016 TECHNICAL DELIVERABLES

07/15/2016 — Suggest steps for optimizing scintillator glass to experimental collaborators
09/30/2016 — Deliver report on chemical/process/composition trends of glass hosts for scintillators to NA-22

FY 2016 TECHNICAL MILESTONES

03/01/2016 — Establish experimental collaboration to test predictions
01/30/2016 — Compare effects of composition on atomic and electronic structure of glasses
06/30/2016 — Determine electronic transport coefficients for modeled glass structures

Task 9: **Evaluate carrier trapping contributions from dislocations and "decoration" (impurities, precipitates)**
This task will use a multi-scale dislocation model, the electronic properties of dislocations determined in the first years of this project, and incorporate known

electronic properties of impurities and precipitates to deconvolve the impact on carrier transport of a bare dislocation network *vs.* decorated dislocations.

FY 2016 Technical Deliverables

09/30/2016 — Submit manuscript on electronic properties of dislocation networks in CdTe to peer-reviewed journal

FY 2016 Technical Milestones

03/30/2016 — Evaluate electronic properties of key impurities embedded in a straight dislocation core
07/15/2016 — Use simulations along with experimental data to evaluate contributions of bare and decorated dislocations on carrier transport in CdTe

Summary Table of Milestones and Deliverables for FY2014

Highest Value	Due Date	M/D	Task #	Description
	09/30/2014	M	1	Complete construction of atomistic interface model for 1 relevant metal
	09/30/2014	D	2	Deliver report contrasting atomic structure motifs of two glass models and validation data to NA-22
	11/30/2014	M	2	Validate structure and electronic density of states of amorphous silica test-case
	02/15/2014	M	2	Construction of first complete glass model
	03/30/2014	M	2	Analysis of structure factor of model and comparison to experimental data from literature
	08/30/2014	M	2	Completion of two comparative glass models
*	06/30/2014	D	3	Submit manuscript on atomic and electronic structure of straight dislocations in CdTe to a peer-reviewed journal
	01/31/2014	M	3	Obtain electronic gap states of a single straight edge dislocation, as a function of distance from the core
	03/30/2014	M	3	Use empirical potentials combined with density functional theory to generate structures and determine the electronic states of a set of at least 6 dislocations in CdTe

** Highest value Milestone or Deliverable (M/D) for each year of the proposal.*

SUMMARY TABLE OF MILESTONES AND DELIVERABLES FOR FY2015

Highest Value	Due Date	M/D	Task #	Description
	09/30/2015	D	1	Deliver report on chemical thermodynamics of TlBr–metal interfaces (at least 2 relevant metals) to NA-22
	02/28/2015	M	1	Complete construction of atomistic interface model for at least 2 relevant metals
	04/30/2015	M	1	Analysis of interface chemical thermodynamics, in terms of stable interface phases
*	09/30/2015	D	4	Deliver report on heterostructure effects on device stability of TlBr detectors to NA-22
	02/15/2015	M	4	Construct interface models with heterostructure material between TlBr and metal
	07/15/2015	M	4	Determine electronic states and Fermi-level pinning of interfaces
	09/30/2015	D	5	Submit manuscript on electronic structure of two glass hosts to peer-reviewed journal
	09/30/2015	D	6	Submit manuscript on atomic and electronic structure of a kinked dislocation in CdTe to a peer-reviewed journal
	01/30/2015	M	6	Use empirical bond-order potential to generate initial structure of a kinked screw
	03/30/2015	M	6	Relax structure of kinked screw dislocation with density functional theory
	07/15/2015	M	6	Evaluate electronic density of states for kinked screw dislocation

** Highest value Milestone or Deliverable (M/D) for each year of the proposal.*

SUMMARY TABLE OF MILESTONES AND DELIVERABLES FOR FY2016

Highest Value	Due Date	M/D	Task #	Description
	05/30/2016	D	7	Deliver candidates for optimal TlBr contact structure/process to RMD and LLNL collaborators
	09/30/2016	D	7	Submit manuscript on improved contact design for TlBr detectors to peer-reviewed journal
	03/30/2016	M	7	Evaluate electrochemical potentials at interfaces from metal work functions
	07/15/2016	D	8	Suggest steps for optimizing scintillator glass to experimental collaborators
*	09/30/2016	D	8	Deliver report on chemical/process/composition trends of glass hosts for scintillators to NA-22
	03/01/2016	M	8	Establish experimental collaboration to test predictions
	01/30/2016	M	8	Compare effects of composition on atomic and electronic structure of glasses
	06/30/2016	M	8	Determine electronic transport coefficients for modeled glass structures
	09/30/2016	D	9	Submit manuscript on electronic properties of dislocation networks in CdTe to peer-reviewed journal
	03/30/2016	M	9	Evaluate electronic properties of key impurities in straight dislocation core
	07/15/2016	M	9	Use experimental data along with simulations to evaluate contributions of bare and decorated dislocations on carrier transport in CdTe

** Highest value Milestone or Deliverable (M/D) for each year of the proposal.*

OFFICE OF DEFENSE NUCLEAR NONPROLIFERATION RESEARCH & DEVELOPMENT

QUARTERLY PROGRESS REPORT FOR THE PERIOD OCTOBER – DECEMBER 2013

PROJECT TITLE: Materials Modeling for High-Performance Radiation Detectors

webPMIS PROJECT NUMBER: LL13-MatModelRadDetect-PD2Jf LAB/CONTRACTOR: LLNL

B&R CODE: NN2001-02 DATE: January 20, 2014

PRINCIPAL INVESTIGATOR:	Vince Lordi, 925-423-2755
LLNL PROJECT MANAGER:	Stephen A. Payne, 925-423-0570
LLNL POINT OF CONTACT:	Jenni Pruneda, 925-422-3037
HQ TEAM LEAD:	David B. Beach, 202-586-0346
HQ OFFICE MANAGER:	David A. LaGraffe, 202-586-1928

PROGRESS (BY TASK) DURING QUARTER:

Task 1: Build atomistic chemical models of TlBr–metal interface

Upcoming milestones:
09/30/2014 — Complete construction of atomistic interface model for 1 relevant metal

Most work on this task is scheduled to begin in Q3 FY14, so little effort was spent on this task during Q1.

Nonetheless, some effort was expended to calculate the electron affinity of TlBr, since no reliable experimental data is available. This quantity is important to understand how the work function of different possible contact metals line up with the band structure of TlBr, which in turn affects (i) surface accumulation or depletion and/or band bending, and (ii) electrochemical potential available for surface reactions. A recent experimental measurement was attempted by one of our collaborators (A. Nelson, LLNL), but the sample was polycrystalline in nature and the measurement noise was too large to obtain a conclusive value.

Formally, the ionization potential (IP) is the energy difference between the valence band maximum (VBM) and the vacuum level, or the energy required to remove an electron from the sample. In practice, this property is a surface sensitive quantity and depends on the particular surface orientation of the sample. In addition to this anisotropy, for TlBr an additional complicating factor is that some surfaces are polar. Nonetheless, the IP can be calculated by creating a surface slab model and computing the change in average electrostatic potential across the interface into vacuum, with reference to the energy of the VBM.

We computed the IP for two surfaces of TlBr: the polar (100) surface and the non-polar (110) surface, using 4x1 slab supercells with 15–20 Å of vacuum and the PBE exchange-correlation functional. The results are summarized in Table 1, where the range given for the (100) surface reflects computational uncertainties that arise from the polar nature of that surface. The rows labeled "bulk average" reflect a calculation using a bulk approximation for the IP based on the position of the H charge neutrality level compared to the known experimental IP for H_2. That calculation is much cheaper computationally than the slab calculations, but is not surface dependent and in principle represents an average over the different crystal facets. However, the similarity of that result reaffirms the slab results, given the consistency of the results from the two independent methods.

Table 1: Calculated ionization potential for TlBr

Surface orientation	Ionization Potential (eV)
(110)	5.7
(100)	6.3 (5.6 – 7.5)
bulk average (PBE)	5.9
bulk average (HSE06)	6.6

Next quarter, these values will be refined by repeating the calculations with the HSE06 hybrid functional, which better reproduces the band gap of TlBr, but requires significantly more computational time. Only a modest positive correction is expected, since the position of the VBM is fairly well reproduced with PBE. In fact, a test of the HSE06 functional already completed for the "bulk average" method gives a value about 10% higher than the PBE result for that case, as shown in the last row of Table 1, and corrections to the slab results similar to this are expected.

Quantitatively, these results are reasonable and consistent with our knowledge of the behavior of TlBr in devices. An IP around 6–6.5 eV for TlBr places all metal WFs near the center of the TlBr band gap. (The range of metal WFs covers ~4.1 eV [for In] to 5.3 eV [for Pt], with most metals ~4.5 eV.) This lineup implies approximately flat band conditions for TlBr when in contact with a metal.

Task 2: Generate atomistic models for two glass hosts

Upcoming milestones:
11/30/2013 — Validate structure and electronic density of states of amorphous silica test-case
02/15/2014 — Construction of first complete glass model

The overall goal for this task is to establish a computational framework that can mimic a range of experimental glass structures by tuning computational parameters in the construction of the glass model. The motivation is to enable studies of the correlation between atomic structure and electronic transport properties of the glass materials, which translate into correlations between synthesis parameters for a given glass and its transport properties; in addition, studies on compositional dependence of the transport properties of glasses is interesting and relevant (both for choice of glass system and optimization of a given glass system). In the context of scintillator detectors, transport of photogenerated carriers to the activators is a limiting process, particularly in glass hosts where carrier transport in generally poor compared to crystalline hosts. This problem is exacerbated for glasses with low activator solubility (concentration).

The work on this particular task during the past quarter focused on performing validation studies on a well-known system, SiO_2, then beginning the construction of the first glass intended for detailed study, from the sodium silicate system. The $Na_2(SiO_2)_nO$ [sodium silicate] system was chosen since a body of experimental structural information exists for a range of Na compositions and also since it represents a glass system that has been studied for scintillators. While it is not a top-performing glass scintillator host, it will serve as a good benchmark system and given its relation to silica, there is good confidence in the ability to accurately model it's structure.

The first milestone to validate the structure and density of states of amorphous silica was completed. We tested three semi-empirical potentials for structure generation using the melt-quench method: the Tersoff potential, the Garofalini modified BMH 2-body potential, and the Garofalini modified BMH 3-body potential. We implemented the modified BMH 2-body and 3-body potentials in the LAMMPS classical molecular dynamics code to perform the simulations. Previous work has applied the Tersoff potential to simulate the structure of silica glass, and our tests largely agree with that work: while the Tersoff potential yields a reasonable glass structure, it is somewhat over-structured based on comparison to the experimental structure factor [or pair correlation functions g(r)] measured with neutron diffraction. The

Garofalini potentials are more physically-based and fitted over a wide set of glass materials. In general, when the 3-body terms are included they perform better than the Tersoff potential for predicting structure, and also predict a more accurate melting temperature. Figure 1 shows an illustration of the melt-quench glass generation process and a comparison of the g(R) obtained for SiO_2 using the 3-body Garofalini potential in both crystalline and glass form against experimental data.

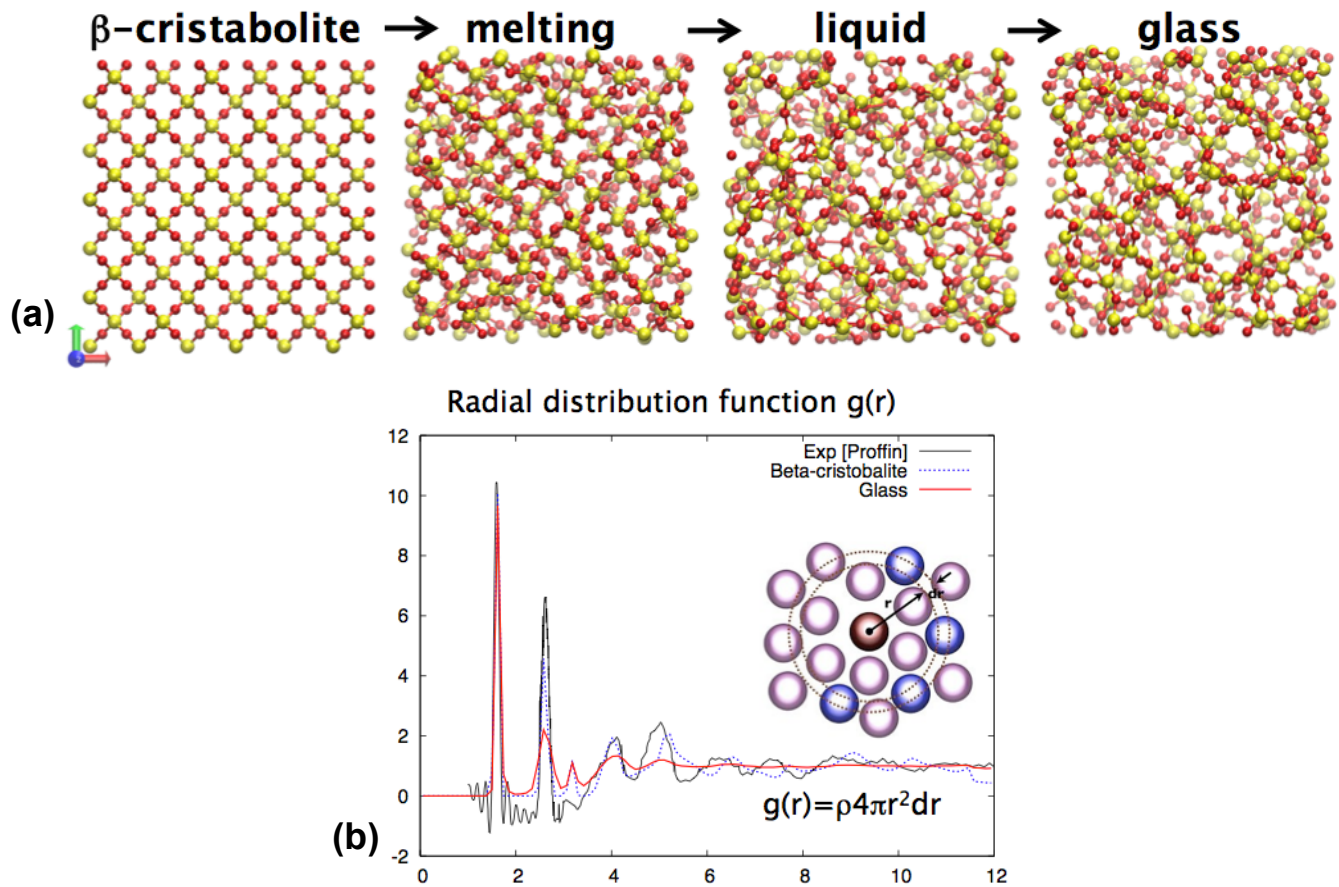

FIG. 1: (a) Amorphous silica is constructed by computationally melting β-cristabolite (a crystalline form of SiO_2) and quenching the melt to room temperature using molecular dynamics. (b) Comparison of radial distribution function g(R) for the crystalline form, the melt-quenched structure, and experimental data for silica from neutron diffraction.

Parameters for 2-body and 3-body terms in the Garofalini potential are available for quite a wide variety of glass compositions that include Si, O, Al, Ca, Na, H, B, and N atoms; potentials for other elements are available in more limited scope.

Snapshots of the glass structure obtained for silica were used to calculate the electronic DOS, shown in Fig. 2. Gap states arising from structural defects are apparent, as expected, showing Anderson localized states at the band edges and a larger mobility gap; the trapped localized states are involved in hopping-like polaronic transport, in agreement with experiment. Structural analysis of the origins of the gap states shows that the states near the valence band maximum are derived from either non-bonded oxygen (nbo) defects or 5-coordinated Si (V-Si) defects. States near the conduction band edge are predominantly associated with 3-coordinated O (III-O) defects. In some structures, deep gap states associated with nbo also appear. (See Fig. 2c.) Further analysis of the localization of states was performed by computing the inverse participation ratio (IPR) for each electronic state. Higher IPR values indicate more localization of a state, so a plot of IPR against the DOS demarcates the localized band tail region against the delocalized band states. Figure 2b shows this analysis for the SiO_2 glass, where localized band tail states near the VBM are most apparent.

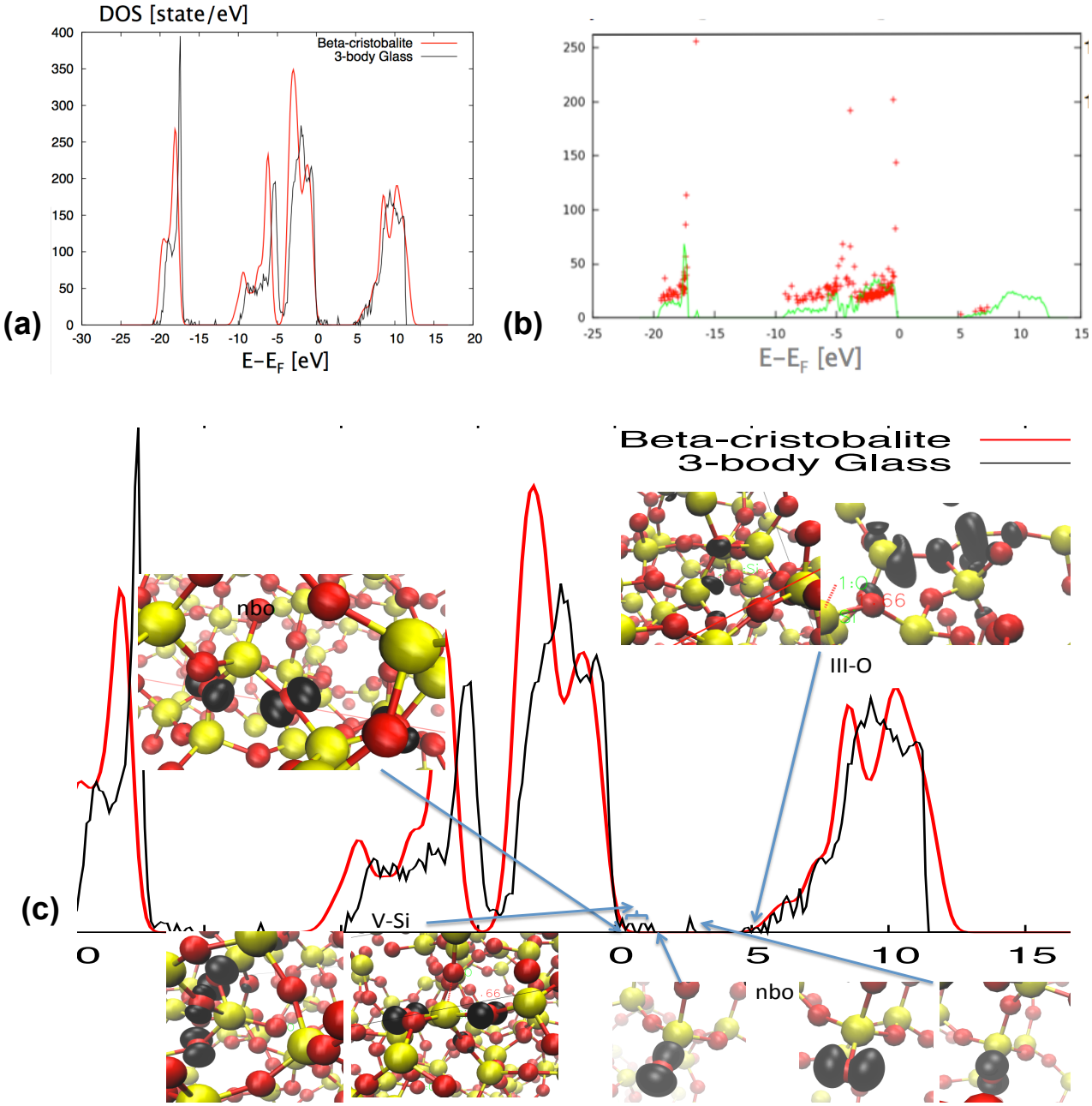

FIG. 2: (a) Electronic density of states (DOS) of crystalline vs amorphous SiO_2, showing band edge and gap states appearing for the amorphous form. (b) IPR (red points) plotted again DOS (green line) for the amorphous structure, showing high degree of localization associated with gap and edge states. (c) Zoom-in of DOS, with isosurfaces of partial charge (in black) plotted for each edge or gap state associated with amorphous structure. The character of each state is labeled as nbo, V-Si, or III-O. (yellow = Si, red = O)

After validation of SiO_2, work on sodium silicate was begun during the quarter and continues into the next quarter. The melt-quench process was completed using a 3-body Garofalini modified BMH potential, for a glass with 30.6% Na_2O. To analyze the electronic properties and statistics in details, we are using a strategy of selecting 30 random snapshots from the molten state, then quenching each to room temperature, from which density functional theory is used to relax to a local minimum and obtain the electronic states. During the quarter, one of these snapshots has been relaxed and analyzed to test the procedure, before repeating on the other snapshots. The structure of the glass [g(R), ring-size statistics, and Q^n number (a measure of bond breaking)] is being analyzed to characterize each snapshot, enabling correlation of atomic structure and electronic structure (DOS, IPR), as well as comparison to experimental structural data. This analysis is ongoing, along with the generation of the additional quench samples. One

technical aspect that is currently being investigated is the appearance of certain melt-quench features that appear to be artifacts, in particular the occasional appearance of ozone molecules within the structure.

Task 3: Build and determine electronic structure of various straight dislocations in CdTe

Upcoming milestones:

01/31/2014 — Obtain electronic gap states of a single straight edge dislocation, as a function of distance from the core

03/30/2014 — Use empirical potentials combined with density functional theory to generate structures and determine the electronic states of a set of at least 6 dislocations in CdTe

For this task, structural models for 7 different straight dislocations in CdTe were generated. Previously, the 8-center Cd-core [-110] edge dislocation structure was completed, and radial-averaged electronic DOS were extracted for that structure, meeting the first milestone for this task. The corresponding 8-center Te-core [-110] edge dislocation was also computed. This quarter, 4 additional core structures for the [-110] edge dislocation were constructed, namely 4-center and 5/7-center structures for both Cd-core and Te-core configurations. In addition, a [-110] screw dislocation was constructed. All structures were created by beginning with an ~18,000 atom slab model of the dislocation (1 unit cell thick), which was relaxed with free boundary conditions using a Stillinger-Weber semi-empirical potential. Then, a hexagonal region ~80 Å in diameter was cut out containing at least ~600 atoms, with boundaries ≥6 unit cells from the core, for further relaxation with density functional theory. (See Fig. 3.) We had previously determined that at least 6 unit cells are required between the core and the edges to ensure the boundary conditions do not affect the electronic density of states or atomic forces in the core region. To transfer the long-range strain from the large semi-empirical model to the smaller DFT model, we fix the positions of the edge atoms (after scaling the lattice constant to the DFT equilibrium value) and also passivate the dangling bonds with pseudo-hydrogen atoms (containing either 1.5 or 0.5 electrons, depending on bond). The cutout is surrounded by at least 20 Å of vacuum region to eliminate image interactions in the periodic DFT calculations. For reference, a correspondingly shaped ideal CdTe structure (containing no dislocation) was also constructed to provide a baseline of the "perfect" crystal DOS.

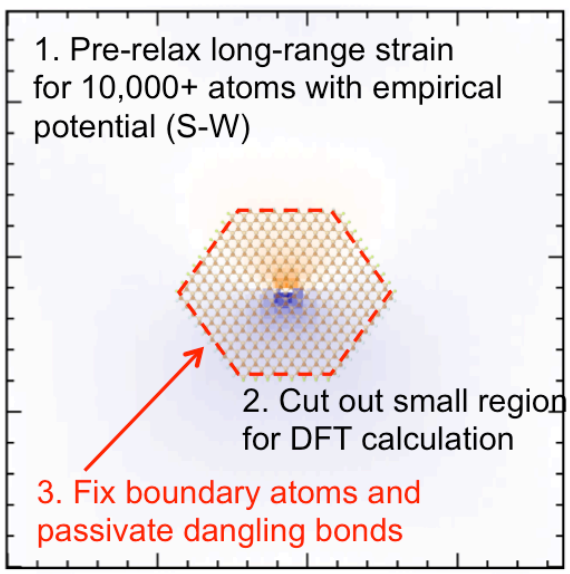

FIG. 3: Illustration of dislocation model construction procedure. A very large model containing a single dislocation core is first relaxed with open boundary conditions using a Stillinger-Weber (S-W) potential. Then a smaller region denoted with the red dashed line is cutout for DFT relaxation. Long-range strain is passed to the smaller model by fixing the edge atoms and passivated the dangling bonds with pseudo-hydrogen atoms. The shading in the figure shows the strain field of the dislocation core, with blue indicating compression and orange indicated tension.

Figure 4 illustrates the core structures of the different dislocation models. All of the models have been relaxed with DFT (local density approximation). Structurally, we find that Cd–Cd dimers in the Cd-core

structures have shorter bond lengths (stronger bonding) than the Te–Te dimers in the Te-core structures. For example, in the 8-center structures, the Cd-core has 3.1 Å Cd–Cd bond length, while the Te-core has 3.7 Å Te–Te bond length. (The ideal Cd–Te bond length is 2.8 Å.)

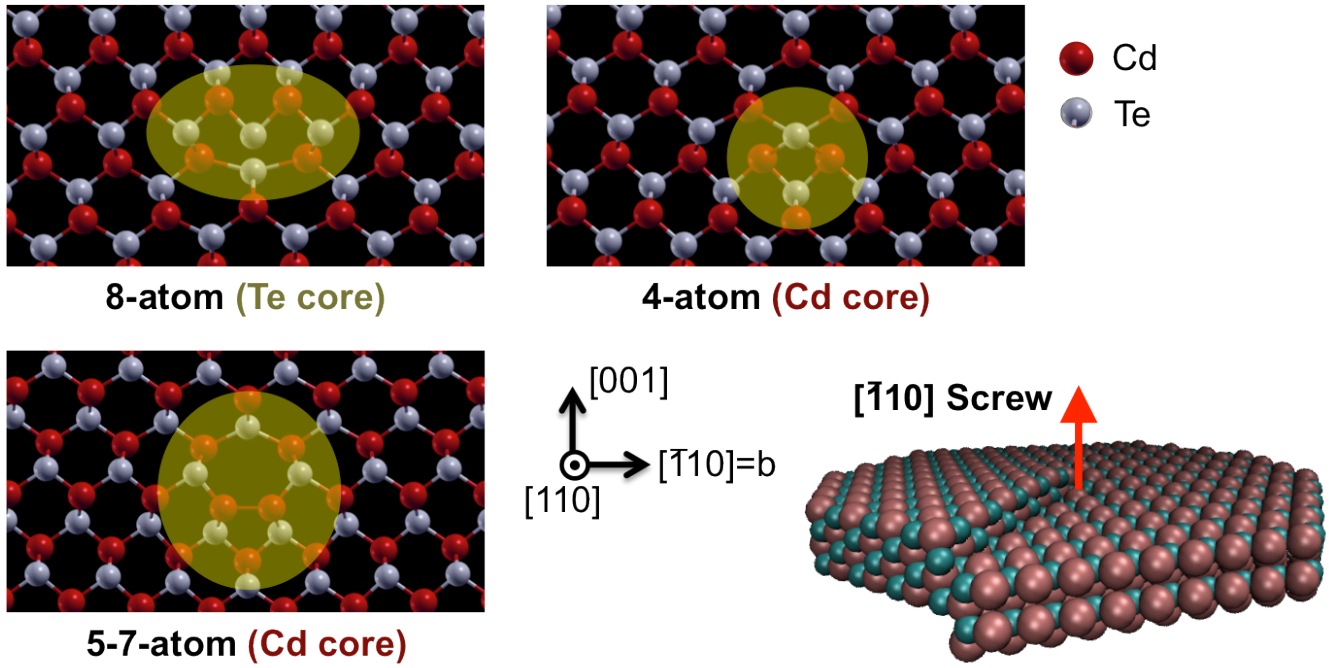

FIG. 4: Illustration of the different core structures considered. The [-110] edge structures are characterized by the size of the rings in the core region (8, 4, or 5/7). Each structure exists in both a Cd-core and Te-core configuration, defined by the dimer created at the center. Only one type is shown here for each structure, for illustration. The [-110] screw structure is also shown.

Electronic DOS analyses for the 8-center Cd-core and Te-core edge dislocations have been completed. Figure 5 shows sample data for the 8-center Cd-core dislocation. Analyses for the other core structures are on-going and will be completed next quarter (3/30/2014 milestone). An analysis framework was developed to extract and plot the electronic DOS as a function of distance from the dislocation core (annular averages), as well as to generate the DOS difference compared to the ideal CdTe structure and to prepare plots of the partial charge densities ("orbitals") for states appearing within the band gap at the core. This framework will be applied to the full set of core structures. In particular, this analysis follows our earlier discovery of a hole trap state for the 8-center Cd-core [-110] edge dislocation with a continuous conducting channel down the dislocation line.

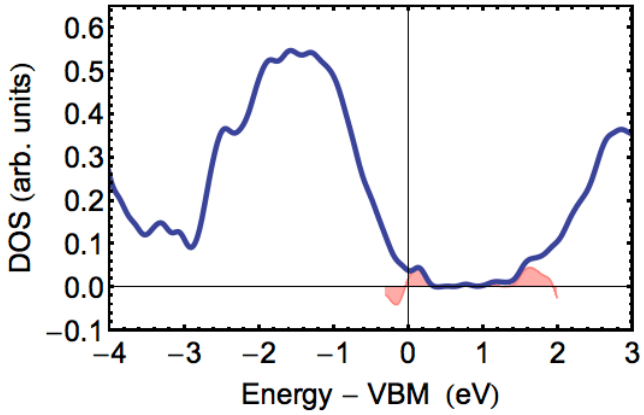

FIG. 5: Electronic density of states localized within 10 Å of the dislocation core for a 8-center Cd-core [-110] edge dislocation. The red shading shows the difference DOS compared to perfect CdTe, highlighting the core gap states due to the dislocation, particularly the hole trap state appearing near the VBM.

COMMENTS (BY TASK):

Planned work for next quarter is as follows.

Task 1: Build atomistic chemical models of TlBr–metal interface

Most work for this task is scheduled to begin in Q3 FY14. However, next quarter, following the work of the past quarter, a small effort will be expended to complete the HSE06 refinements of the ionization potential (IP) calculations. In addition, a summary analysis of our previous results for contact metals will be completed in light of the band lineups resulting from the computed IP and any surface charge accumulation from band bending.

In Q3, we will begin work to compute the thermodynamics of several chemical interphases for a chosen metal.

Task 2: Generate atomistic models for two glass hosts

Work next quarter will focus on completing the structure generation and electronic structure calculations of the sodium silicate glass to meet the second milestone for this task. The quench/anneal cycles will be completed for a series of melt snapshots, to obtain an ensemble of atomic and electronic structures representing the material. The milestone goal is to complete this work for a single glass composition (30.6% Na_2O in sodium silicate), but depending on the rate of progress additional compositions may be tackled as well.

Task 3: Build and determine electronic structure of various straight dislocations in CdTe

During the next quarter, the analysis of the electronic density of states around each of the 7 dislocation models relaxed during the last quarter will be completed. The results will be prepared for presentation at the Materials Research Society Spring Meeting, where our abstract has been accepted for oral presentation, and a manuscript will be prepared for journal publication. In addition, if necessary, select models will be checked against larger DFT models (800 atoms or more) to verify size convergence of the results.

COSTING:

Costing information in webPMIS is current. Spending progress is on par against the cost plan.

MERIT REVIEWED PUBLICATIONS/TECHNICAL REPORTS/OTHER PUBLICATIONS:

N. Adelstein and V. Lordi, "Understanding Conductivity in Glasses via First-Principles Study of Localized States," poster OO3.26 presented at Materials Research Society Fall Meeting, Boston, Dec. 4, 2013.

V. Lordi, D. Åberg, M. Skarlinski, and E. Cho "Atomic and Electronic Structure of Dislocations in CdTe," abstract accepted for presentation H1.10 at Materials Research Society Spring Meeting, April 22, 2014.

OFFICE OF DEFENSE NUCLEAR NONPROLIFERATION RESEARCH & DEVELOPMENT

QUARTERLY PROGRESS REPORT FOR THE PERIOD JANUARY – MARCH 2014

PROJECT TITLE: Materials Modeling for High-Performance Radiation Detectors

webPMIS PROJECT NUMBER: LL13-MatModelRadDetect-PD2Jf LAB/CONTRACTOR: LLNL

B&R CODE: NN2001-02 DATE: March 31, 2014

PRINCIPAL INVESTIGATOR:	Vincenzo Lordi, 925-423-2755
LLNL PROJECT MANAGER:	Stephen A. Payne, 925-423-0570
LLNL POINT OF CONTACT:	Jenni Pruneda, 925-422-3037
HQ TEAM LEAD:	David B. Beach, 202-586-0346
HQ OFFICE MANAGER:	David A. LaGraffe, 202-586-1928

PROGRESS (BY TASK) DURING QUARTER:

Task 1: Build atomistic chemical models of TlBr–metal interface

Upcoming milestones:
09/30/2014 — Complete construction of atomistic interface model for 1 relevant metal

Most work on this task is scheduled to begin in Q3 FY14, but a small effort was spent continuing the work begun in FY14 Q1 on calculating the ionization potential (IP) of TlBr. In Q1, we had computed the IP of two surfaces of TlBr, the polar (100) surface and the non-polar (110) surface, using the PBE exchange-correlation functional and supercell models containing slab and vacuum regions. We had also computed direction averaged "bulk" values using both PBE and HSE functionals, using the "branching-point energy" method associated with the H impurity charge neutrality level. Good agreement between the two methods showed that TlBr has a small direction-dependence of its IP and also that PBE gives a reasonably good result compared to the more accurate, but computationally expensive, HSE x-c functional. During this quarter, we completed the direct calculation of the IP for the non-polar (110) surface using the HSE hybrid functional and a slab/vacuum model, which was an extremely computationally demanding calculation. The result refined our best estimate of the IP (~6.1 eV) and also confirmed the result from the "bulk" method, although the values are not identical, as expected. All of the results are summarized in Fig. 1.

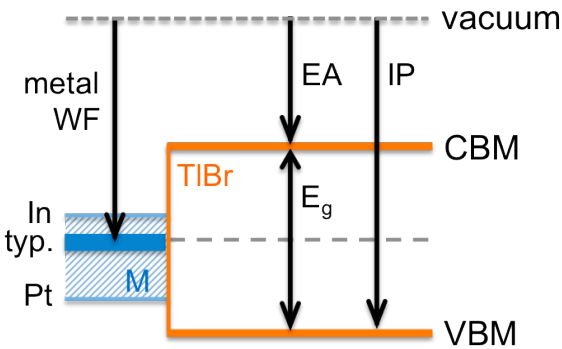

Surface	IP (eV)
(110) [PBE]	5.7
(110) [HSE]	6.1
(100) [PBE]	6.3 – 6.8
bulk average [PBE]	5.9
bulk average [HSE]	6.6

FIGURE 1. (left) Band lineup of metals with TlBr, with schematic definitions of relevant quantities indicated (IP = ionization potential, EA = electron affinity, WF = work function, E_g = band gap). (right) Table summarizing calculated IP for TlBr, using both PBE and HSE exchange-correlation functionals, and comparing direct slab method with the "bulk average" method.

Task 2: Generate atomistic models for two glass hosts

Upcoming and recent milestones/deliverables:
11/30/2013 — Validate structure and electronic density of states of amorphous silica test-case
02/15/2014 — Construction of first complete glass model
03/30/2014 — Analysis of structure factor of model and comparison to experimental data from literature

During this quarter, we focused on constructing validated atomistic models of sodium silicate glass using melt-quench-anneal simulations with semi-empirical potentials. The resulting structures were validated against available neutron diffraction data from the literature; we also worked to validate the potentials used. The chosen test glass (sodium silicate) is formally composed of a mixture of Na_2O and SiO_2 fragments. We worked with compositions given by the ratio of Na_2O:SiO_2 of 1:2, 1:3, and 3:7. The initial structures are generally built starting from a crystalline form of SiO_2 and replacing random moieties of SiO_2 with Na_2O before melting. However, tests comprised of initially placing the appropriate stoichiometry of all atoms in a supercell randomly yielded identical results, and the initial conditions do not sensitively affect the resulting structures. Ultimately, we are interested in correlating changes in electronic structure with different local chemical environments and density of "defects" produced by glass additives, such as sodium. In particular, we wish to associate different types of structural defects with various localized band tail states in the gap and also possible process variations. In this quarter, we focused simply on structure, with the consequent electronic properties to be investigated later.

We used a 3-body modified-BMH potential provided by Prof. Garofalini (Rutgers) to generate the glass structures. We implemented this potential in the LAMMPS molecular dynamics code. Two sets of parameters were available, so we compared the results using each, as well as the results using a different potential from the literature due to Yuan and Cormack (2001). More details of melt-quench parameters and procedure are given below, but for these comparisons several different parameters were tested, with little sensitivity. For example, quenches from 8000 to 300 K or 5000 to 300 K were used, with quench rates between 5 and 100 K/ps. Molecular dynamics time steps of 1 or 2 fs were used. Experimental densities of 2.4–2.5 g/cm^3 were used with boxes containing ~800–1500 atoms. (We desire to keep our atom count low enough to be able to run DFT-based electronic structure calculations on the same systems later.) The results of these tests are summarized in Fig. 2, which shows the total pair distribution function obtained from the revised Garofalini potential ("E-glass"), a previous version of the potential ("Melman 1991"), the "Cormack" potential, and neutron diffraction data from Wright. While the Yuan-Cormack potential agrees slightly better with the experimental data at short range, the Garofalini potentials match the mid-range order better. Tests with 1500-atom and 648-atom supercells showed that the cell size had little effect on the results.

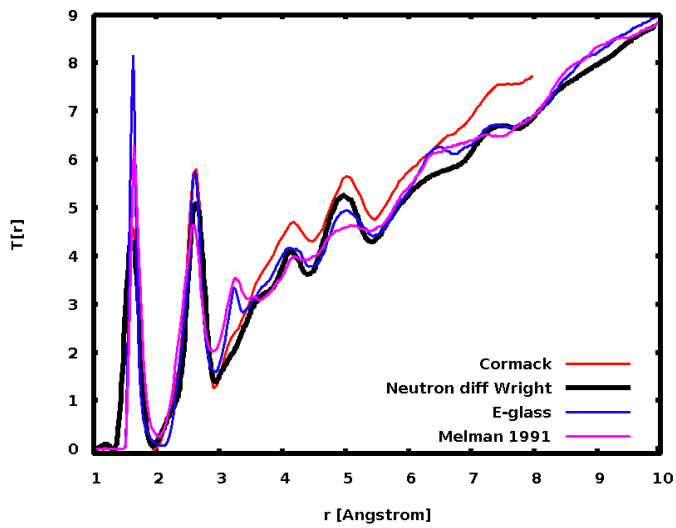

FIGURE 2. Total pair distribution function $T(r)$ for 3:7 (Na_2O:SiO_2) sodium silicate glass (768 total atoms) obtained from melt-quench with different potentials (thin colored lines), compared to experimental neutral diffraction data (thick black line).

We then studied the effect of quench rate on the obtained structure, over 4 orders of magnitude from 0.01 to 100 K/ps. The fastest quench rate (100 K/ps) resulted in obvious over-structuring of the glass, with sharper short-range peaks in the pair distribution function compared to experiment. Good agreement with experiment was achieved with the slower quench rates, with little difference between 0.01 and 0.1 K/ps. Thus, 0.1 K/ps seems like an optimal quench rate for structure generation.

Finally, a number of tools were established for the quantitative analysis of glass structures, including local "defects." One metric of the glass structure is ring statistics, which counts the number of rings of a given size in a structure, where rings are defined locally by the smallest connected loop of Si atoms. Another important structural parameter is the Q^n number, which is defined to measure the number of non-bridging oxygen (nbo) atoms bound to a given Si atom: for a given Si atom with y nbo defects in a silicate, $n = 4 - y$. Non-bridging oxygens are those that are bonded to only one Si atom. We have tested tools in place to perform averaged ring counting using the Franzblau procedure and to compute averaged statistics of Q^n numbers. In addition, we compute total and partial structure factors, for which some examples are given above with total pair distribution functions; various other pair distribution functions can be computed as well.

A full comparison of the resulting structures from different melt-quench-anneal procedures, using the quantitative structure characterization tools described above, will be performed next quarter to better assess the variability among structures. Then, the electronic structure will be evaluated with density functional theory and correlated to the local structural motifs in the glasses. However, initial application of the Q^n analysis revealed a curious discrepancy in some of the potential parameters used, which requires further investigation. In particular, for tests on silica using the modified-BMH potential form, parameters taken from "Melman 1991" give very different Q^n results than expected (in disagreement with reported values in the original paper), despite agreement of the pair distributions, which albeit are a less sensitive measure. As shown in Table 1, updated parameters received through private communication give better results, but still show significant discrepancies.

	Melman original	**Melman repeat**	**Private commun.**
Q^4	31.0 %	71 %	44 %
Q^3	44.1	29	35
Q^2	10.7	0	7
Q^1	0	0	2
Q^0	0	0	1

TABLE 1. Distribution of Q^n in silica test system with two version of modified-BMH

potential, compared to original paper.

Task 3: Build and determine electronic structure of various straight dislocations in CdTe

Upcoming and recent milestones/deliverables:
01/31/2014 — Obtain electronic gap states of a single straight edge dislocation, as a function of distance from the core
03/30/2014 — Use empirical potentials combined with density functional theory to generate structures and determine the electronic states of a set of at least 6 dislocations in CdTe

Following on the work from last quarter, the electronic density of states as a function of distance from dislocation core were analyzed for the full set of 6 edge dislocations and 1 screw dislocation. The set of dislocations studied was described in the FY14 Q1 report and consists of [-110] dislocations, which is the favorable dislocation direction in CdTe. Three different edge dislocation core structures were studied, denoted 8-core, 5-7-core, and 4-core, to correspond to the core symmetry. For each core structure, Cd-core and Te-core structures are possible, depending on which element dimerizes in the core. The screw dislocation studied was also oriented along [-110].

The stability of each core structure was compared by computing the energy per length of each dislocation model. The results are summarized in Table 2. Overall, the screw dislocation is the most stable, since there are no wrong-bonds in the structure. Among the Te-core structures, the Te 5-7 core is most stable; among Cd-core, the Cd 8-core is most stable. In general, Te-core structures are favorable over Cd-core structures and 4-core structures are not preferred.

Dislocation Structure	Relative Formation Energy (eV/nm)
Cd 4-core	5.60
Cd 5-7-core	4.02
Cd 8-core	**3.46**
Te 4-core	3.23
Te 5-7-core	**0.00**
Te 8-core	1.67
Screw	**–33.9**

TABLE 2. Relative energies of dislocation structures studied.

The electronic properties of each core structures was analyzed by plotting the integrated electronic density of states (DOS) in successive annuli around the core, to determine the DOS as a function of distance from the core. This allows variations with distance to be studied, as well as determine the extent of electronic variations due to the dislocation core structure. In addition, structure validation is possible by confirming that each model contains an effective "bulk" region shielding the core electronic structure from any edge effects, as described in the FY14 Q1 report. In general, we find the electronic structure of the core region to extend ~10 Å radius from its center, as illustrated in Figure 3.

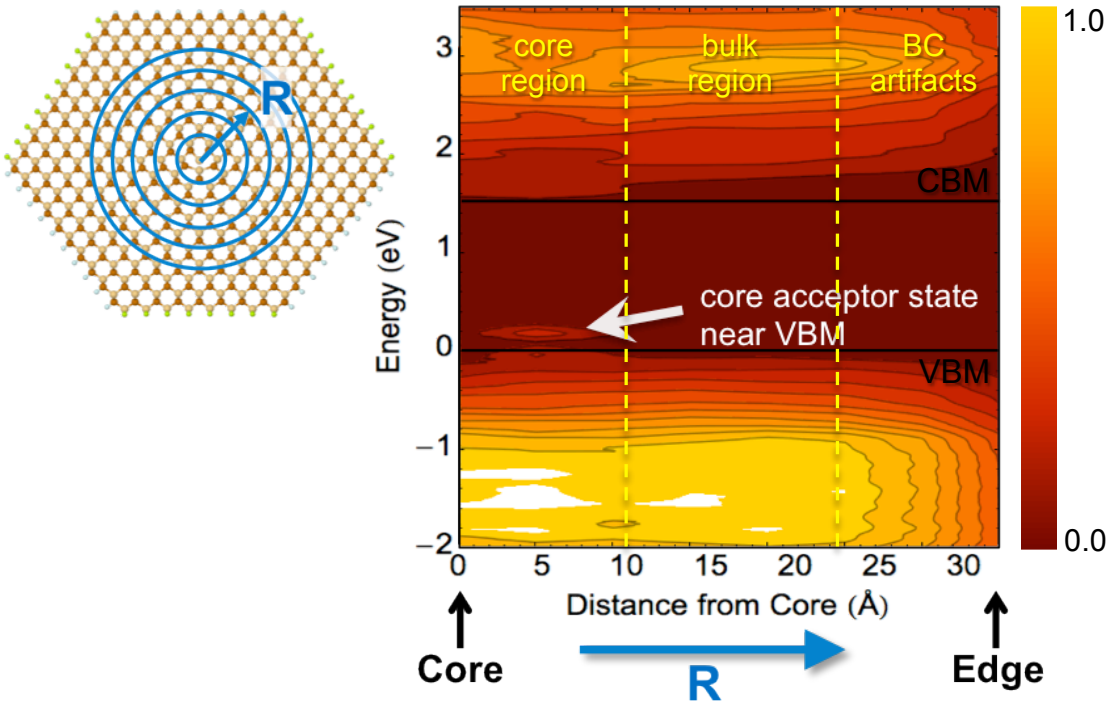

FIGURE 3. Electronic density of states of Cd-8-core edge dislocation as a function of distance from center of core. The core region is within 10 Å from the center, and a bulk-like region is apparent between ~10 and 25 Å, while edge effects from the model are evident beyond 25 Å.

We then plot the integrated DOS of each core (within 10 Å radius) along with the bulk CdTe DOS without any dislocation, to identify features associated with the dislocations (Fig. 4). In general, the findings include that: (i) 8-core edges exhibit a gap state near the VBM, (ii) 5-7-core edges exhibit a deep mid-gap state, and (iii) the screw dislocation does not introduce any gap states, but new states above the CBM, within the conduction band. The 8-core structures also show states above the CBM, with those for the Cd-core being closer to the CBM than the Te-core. In addition, we find that the acceptor state induced near the VBM for the 8-core structures introduce a conducting channel down the dislocation line. For the 8-cores, the Cd-core also is characterized by a state near the CBM, while the Te-core is associated with a depletion of the top of the valence band compared to bulk CdTe.

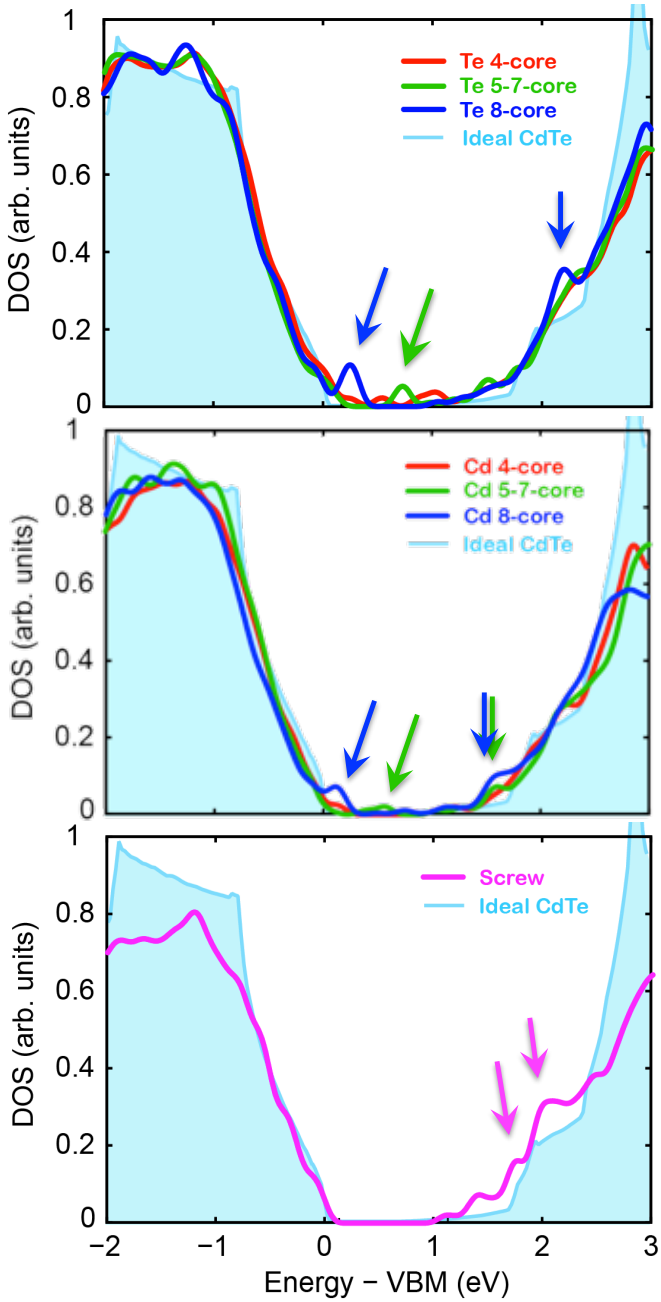

FIGURE 4. Dislocation core DOS (lines), integrated within 10 Å radius from the center, compared to bulk CdTe DOS (light blue shading). The data are grouped by Te-core structures (top panel), Cd-core structures (middle panel), and screw (bottom panel). Arrows highlight core-related electronic states of particular note.

COMMENTS (BY TASK):

We have a staffing need for a new postdoc dedicated to TlBr tasks in this project, slated to begin in earnest in FY2014 Q3. During this quarter we have interviewed several excellent candidates from UC Berkeley and the University of Texas. We intend to make a new hire by Q3. In the meantime, we have utilized a fraction of an existing postdoc (Joel Varley) very effectively in this role. We currently have dedicated staff in place for the other tasks.

Planned work for next quarter is as follows.

Task 1: Build atomistic chemical models of TlBr–metal interface

In FY14 Q3, we will begin investigation of chemical compounds related to the contact layer of TlBr detectors. The first compound we plan to investigate is the TlBrCl alloy, which may be formed by chlorination of the surface of TlBr. Early experiments by our collaborators suggest that such Cl treatment may be associated with increased longevity of detectors at room temperature.

Task 2: Generate atomistic models for two glass hosts

In the next quarter, we will seek to resolve the possible issues discovered with the E-glass potential parameters resulting in unexpected Q^n distributions. We will further validate the glass structures against experiments and previous calculations (where available) using sensitive structure metrics, such as Q^n distribution, fraction of nbo's, and ring statistics. We then will generate a large ensemble of structures (30-50) to represent the macroscopic features of a sodium silicate glass using modest-sized supercells appropriate for electronic structure calculations (< 1000 atoms). The electronic structure will be analyzed by computing the localization of states around the gap region, using the inverse participation ratio (IPR) metric. The electronic and atomic structures will be correlated. Variations in generated glass structures, measured with Q^n distribution, ring statistics, etc., will be studied as quench parameters are varied.

Task 3: Build and determine electronic structure of various straight dislocations in CdTe

The calculations and analysis for this task were completed during this quarter, as planned. In the next quarter we will allocate some effort to preparing reports (conference presentations and a manuscript) summarizing the results.

COSTING:

Costing information in webPMIS is current. Spending progress is on par against the cost plan.

MERIT REVIEWED PUBLICATIONS/TECHNICAL REPORTS/OTHER PUBLICATIONS:

No publications.

OFFICE OF DEFENSE NUCLEAR NONPROLIFERATION RESEARCH & DEVELOPMENT

QUARTERLY PROGRESS REPORT FOR THE PERIOD APRIL – JUNE 2014

PROJECT TITLE: Materials Modeling for High-Performance Radiation Detectors

webPMIS PROJECT NUMBER: LL13-MatModelRadDetect-PD2Jf LAB/CONTRACTOR: LLNL

B&R CODE: NN2001-02 DATE: June 30, 2014

PRINCIPAL INVESTIGATOR:	Vincenzo Lordi, 925-423-2755
LLNL PROJECT MANAGER:	Stephen A. Payne, 925-423-0570
LLNL POINT OF CONTACT:	Jenni Pruneda, 925-422-3037
HQ TEAM LEAD:	David B. Beach, 202-586-0346
HQ OFFICE MANAGER:	David A. LaGraffe, 202-586-1928

PROGRESS (BY TASK) DURING QUARTER:

Task 1: Build atomistic chemical models of TlBr–metal interface

Upcoming milestones:
09/30/2014 — Complete construction of atomistic interface model for 1 relevant metal

During this quarter, we focused on an experimentally-relevant chemical compound associated with the TlBr contacts, motivated by results from our experimental collaborators (A. Conway, *et al.* at LLNL and K. Shah, *et al.* at RMD; DNDO-funded project PI: A. Conway). Recently, A. Conway, *et al.* have found that surface treatment with HCl has improved the longevity of TlBr gamma detectors at room temperature. The surface treatment was found to form a chlorinated alloy of $TlBr_{1-x}Cl_x$ at the surface, with the Cl content variable depending on process conditions. The reason for the device improvement with chlorination is not understood, and the mechanism could shed important light on material parameters (electronic or otherwise) relevant to optimizing the contact stack.

Our work during this quarter began to address two aspects of the TlBrCl alloy of potential relevance: the electronic properties and the diffusive properties.

We first sought to understand how the band edges of TlBr and TlBrCl align, which could be important for charge transport and blocking of contact injection current, since the band gap of TlCl (~3.2 eV) is larger than TlBr (2.7 eV). To this end, we computed the valence band offset (VBO) between TlBr and TlCl, using the accurate HSE hybrid functional and various methods. Slab models consisting of alternating layers of TlBr and TlCl (oriented along [110]) with optimized interface spacing and straining the TlCl onto the TlBr "substrate" were used, and compared with calculations based on "branching point energy" (H impurity charge neutrality levels in bulk calculations). As for the IP calculations of last quarter, good agreement among the methods was obtained, for high confidence of the calculations. The result was a computed VBO of –0.41 eV for TlCl relative to TlBr, which implies a CBO ~0.1 eV (or slightly higher). Thus, at least for the pure end compounds, the presence of a TlCl layer on top of TlBr may present a hole barrier, but not an electron barrier. In the next quarter, we plan to extend the analysis across the composition range of $TlBr_{1-x}Cl_x$. We also compared our result to preliminary measurements of the band offset using x-ray photoemission spectroscopy (XPS). The measurement interpretation and error analysis

still requires some refinement, but the preliminary measured VBO was ~ –0.5 eV, close to our computed value.

Electrical properties associated with a surface layer, such as the band offsets and trap levels, may be important to device operation and predicting longevity, but physical effects may be important as well. For example, a surface compound may have particular properties promoting or diminishing vacancy migration or injection, or be a source of or blocking layer for mobile impurities that may inject carrier traps or charges into the active region. Either of these scenarios can contribute to time-dependent detector performance enhancing or degrading longevity. In this context, we computed the migration barriers for vacancy motion in TlBr and TlCl; we also repeated the calculations as a function of lattice constant ranging over the values for TlBr to TlCl, to model variations with composition and lattice strain. In addition, we computed the barriers for migration of Br in TlCl and Cl in TlBr over the same range of conditions, to understand the propensity for and the relative rates of intermixing under a driving force. By combining the results of these calculations, the data shown in Fig. 1 were generated. Fig. 1 shows the computed migration barriers of each anion in the alloy across the composition range of TlBrCl, assuming a vacancy hop mechanism. The end points (0 and 100%) indicate the native anion migration barriers, as well as the barriers for migration of a dilute impurity of the opposite anion (*e.g.*, Cl in TlBr).

The results suggest that Cl mobility is higher regardless of composition and that Cl in TlBr moves faster than Br. We are still analyzing these results in light of experimental observations of composition evolution during detector operation and an associated rate of failure. We will use these data in a finite element diffusion model to attempt to develop a mechanistic understanding of such evolution and device failure, which is currently lacking.

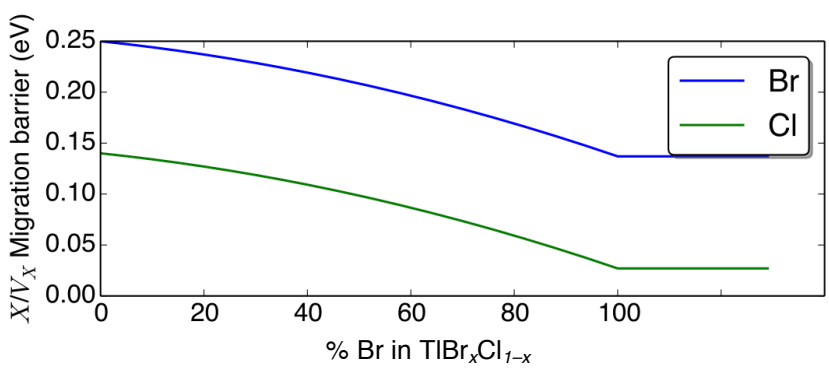

FIGURE 1. Theoretical migration barriers for anions (Br^- or Cl^-) as a function of concentration in TlBrCl alloys.

In addition, the Tl vacancy migration rate as a function of Cl content in TlBrCl is relevant to the rate of migration of metal impurities, which can enter either on the Tl site or as interstitials. Our calculated migration barrier for V_{Tl} is 10% higher in TlCl (0.42 eV) compared to TlBr (0.38 eV), but the small absolute difference (0.04 eV) needs to be verified, since it is near the precision of the calculations. A slightly higher value would suggest that TlCl can form a barrier to injection of some metal impurities from the contacts.

Task 2: Generate atomistic models for two glass hosts

Upcoming and recent milestones/deliverables:
02/15/2014 — Construction of first complete glass model
03/30/2014 — Analysis of structure factor of model and comparison to experimental data from literature
08/30/2014 — Completion of two comparative glass models
09/30/2014 — Deliver report contrasting atomic structure motifs of two glass models and validation data to NA-22

Last quarter a possible problem with potential parameters for sodium silicate was discovered. During this quarter, the potential was corrected and verified. Statistical analysis tools were completed and used validate simulations against experiment. Analysis of the electronic structure of the first glass model was

begun and nearly completed An ensemble of 50 structures of 30:70 Na_2O-SiO_2 sodium silicate glass was relaxed with DFT-PBE to generate electronic density of states, and the IPR were computed to analyze the electronic structure in terms of localization of states in the band tails and in the gap. A summer student began work in mid-June investigating how tuning the melt-quench-anneal procedure affects the number of defects in the resulting glass model. Details follow.

Potential Parameters

The potentials used in this study (referred to as "E-glass") are from a private communication with Prof. Stephen Garofalini of Rutgers University; the potential form, which includes 2- and 3-body terms, is a modified form of the BMH potential and is presented in a paper by Feuston and Garofalini.[1] We discovered that the original published parameters included some typographical errors and also found slight inconsistencies between some versions of the potentials; however, we were able to identify and correct the errors after meeting with Prof. Garofalini at the MRS Spring Meeting in April. We tested the revised potential and also a related potential from the literature[2] ("Melman") against published results for sodium disilicate, using identical setups for the density, number of atoms, and melt-quench procedure from the literature. We used 170 Na atoms, 427 O atoms, and 171 Si atoms in a box size of 27.47 x 27.47 x 13.735 $Å^3$. The box was expanded by 16% for melting, to account for thermal expansion, and then reduced in size over 10 steps during the quench to get back to the room temperature density, given by the box dimensions above. Fig. 2(a) shows that the radial distribution function (rdf) from the Melman paper compares well to the rdf from our simulation using the same parameters; the revised E-glass parameters give slightly different results, but also agree slightly better with experiment (not shown here). We also verified excellent agreement of the Si–O–Si angular distribution, as shown in Fig. 2(b). Furthermore, the more sensitive metrics of Q^n distribution and fraction of non-bridging oxygen (nbo) atoms also agreed well, as shown in Table 1. Hence, we resolved the potential issues and established a validated potential for sodium silicate.

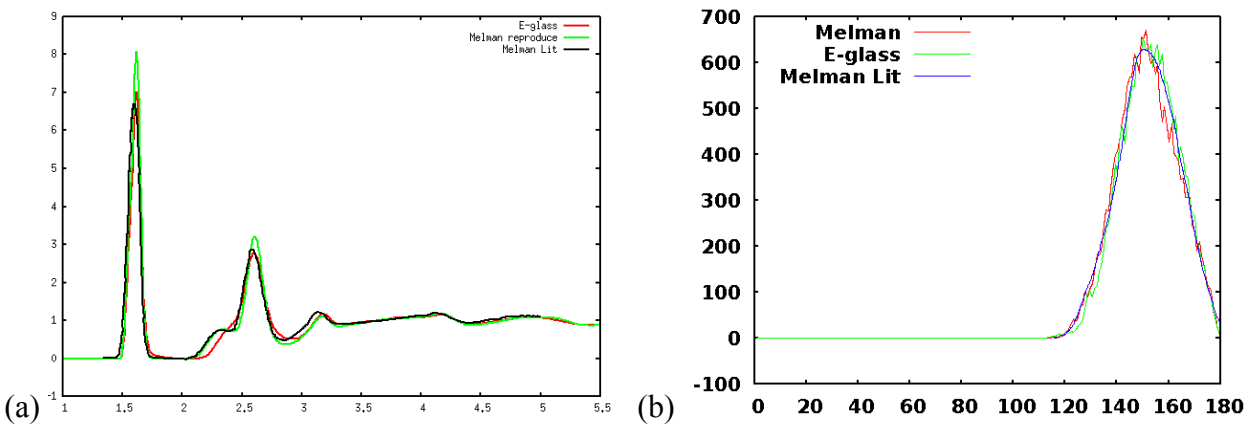

FIGURE 2. (a) Radial distribution function of sodium disilicate from simulations using revised E-glass parameters compared to the corrected parameters from Melman and Garofalini. (b) The angular distribution of Si–O–Si bonds in the same simulations.

[1] B. P. Feuston and S. H. Garofalini, The Journal of Chemical Physics 89, 5818 (1988).
[2] H. Melman and S. H. Garofalini, Journal of Non-Crystalline Solids 134, 107 (1991).

Q^n species % sodium disil.	Melman Literature	Melman	E-glass
Q^4	31.0	30.9	33
Q^3	44.6	42.7	41.4
Q^2	20.2	24.0	23.1
Q^1	4.1	2.36	2.5
Q^0	0	0	0
% nbo	38	38.75	37.7

TABLE 1. Validation of distribution of Q^n and fraction of nbo for sodium disilicate simulations from Fig. 1.

Details of Glass Model Generation Procedure

The glass forming procedure starts with swapping out Si and O atoms for Na from a 4x4x4 β-cristobalite cell and setting the volume to correspond to the experimental density of 2.466 g/cm^3. Molecular dynamics are run using a time step of 1 fs and a Langevin thermostat. First, the structure is minimized at 0 K, and then the temperature is increased from 0 to 8000 K while the volume is scaled up by 16.7% to account for thermal expansion. After equilibrating at 8000 K, a snapshot is taken every 32,000 steps (32 ps) to seed an ensemble of glass structures. Each melt snapshot is quenched to 300 K over 80,000 steps (80ps) while rescaling the volume every 8000 steps, which is equivalent to a quench rate of ~10^{14} K/s. While this quench rate is somewhat fast, it allows comparison to previous similar work in the literature and also gives defect concentrations similar to experiment. Finally, each quenched snapshot is equilibrated at 300 K for 80 ps, during which structural statistics are accumulated.

We chose to simulate the 30:70 Na_2O-SiO_2, to verify our potentials and glass forming methodology. We also compared to a 2001 study[3], which used only 90 atoms (compared to our 660) to simulate the glass and used a different variable charge BKS classical potential. We also compared our results to slower quench rates.

Analysis Tools and Results

There are a variety of ways to characterize an amorphous structure and assess its correspondence to experimentally realized glasses. One of the simplest measures, the radial distribution function (rdf), unfortunately is not very sensitive to subtleties in the structure, so additional metrics are needed. Through NMR and neutron diffraction experiments, the number of non-bridging oxygen (nbo) atoms can be determined. In addition, the average number of nbo connected to each Si atom (related to the Q^n number) and the ring structure can also be determined. Various experimental techniques, including X-ray and neutron diffraction, are sensitive to angular distributions, which comprise further comparative metrics for simulated structures.

In simulations, the sample volume is generally small compared to macroscopic experimental samples. Thus, an adequate sampling of the amorphous structure over macroscopic length scales requires averaging the simulations over an ensemble of "snapshots." With molecular dynamics, these snapshots may be obtained by sampling the dynamics periodically, with the period chosen longer than the timescale of dynamic correlations. This relies on the ergodicity principle of the equivalence of time and spatial averages of the ensemble. We have developed tools to perform these analyses automatically during structure generation, and here show the validation data obtained from the first production runs of 3:7 sodium silicate glass.

[3] X. Yuan and A. N. Cormack, Journal of Non-Crystalline Solids 283, 69 (2001).

a) Radial distribution functions

Various radial distribution functions can be computed. The total correlation function, T(r), is useful for direct comparison of simulated structures to neutron diffraction data, since the broadening function required to account for the experimental neutron scattering length is symmetric and *r* independent, making the broadening relatively simple to implement. The resulting broadened distributions compare very well to experimental data, much better than standard rdf, such as shown in Fig. 2(a) above.

Then, the quality of the simulation compared to a given experiment can readily be quantified by taking the mean square deviation across T(r), via

$$R_\chi = \left(\frac{\sum_i \left[T_{\exp}(r_i) - T_{sim}(r_i) \right]^2}{\sum_i T_{\exp}^2(r_i)} \right)^{1/2}.$$

In Table 2 we show the $R\chi$ values for the three different potentials tested above (Cormack BKS, E-glass, and Melman) computed against to two different experimental data sets by Wright[4] and Johnson.[5] According to these results, the BKS potential performed slightly better than E-glass, however, we have chosen to use the E-glass potential, since it performs reasonably well and since the variable charge in the BKS potential will be difficult to use in multicomponent glasses moving forward. Figure 3 shows a representative T(r) comparison between simulation and experiment for the E-glass potential.

Potential	Wright	Johnson
BKS (Yuan-Cormack)	13.2 %	12.5 %
E-glass	18.9	18.4
Melman	20.6	19.8

TABLE 2. $R\chi$ values for 3:7 sodium silicate simulated structures generated with 3 different potentials (BKS, E-glass, Melman) compared against 2 different experimental neutron diffraction data sets (Wright, Johnson).

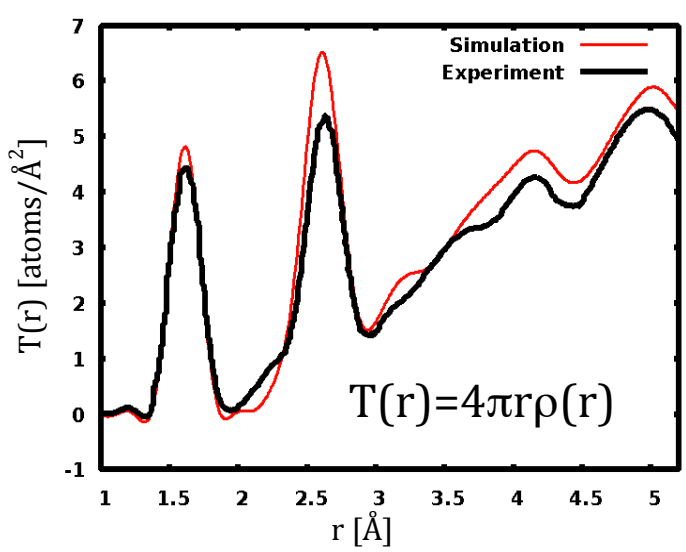

FIGURE 3. Comparison of broadened T(r) from "E-glass" simulation to Wright experimental data.

[4] A. C. Wright, Journal of Non-Crystalline Solids 159, 264 (1993).
[5] J. A. Johnson, C. E. Johnson, D. Holland, A. Mekki, P. Appleyard, and M. F. Thomas, Journal of Non-Crystalline Solids 246, 104 (1999).

b) Non-bridging oxygens, Q^n numbers, and coordination number

Previous studies of silica and sodium silicates have determined that the three main defects are nbo, 5 coordinated Si atoms (V-Si), and 3 coordinated oxygen atoms (III-O). The total number of nbo affects the distribution of Q^n. The distribution of Q^n is a particularly sensitive metric to determine the fidelity of a glass model. In Table 3, we show the distribution of Q^n and the fraction of nbo in our model compared to experimental results. The experiments, however, were for a slightly different glass composition (22.5:77.5 Na_2O:SiO_2, compared to our 30:70). The simulated structure shows a smaller fraction of Q^3 compared to the experiment and a correspondingly larger fraction of Q^2. This is consistent with an increase in nbo, as seen in the table, and is somewhat expected for the larger ratio of Na to Si atoms in the simulated glass. Other simulated structures in the literature, for similar types of glasses, have shown comparable results of lower Q^3/higher Q^2 compared to experiment.[6,7]

	Experiment[8] (22.5:77.5)	**Simulation (E-glass) (30:70)**
% nbo	28 %	34.0 ± 0.4 %
% Q^4	37.2 %	37.4 ± 1.9 %
% Q^3	60.5	44.8 ± 3.5
% Q^2	2.3	15.6 ± 2.3
% Q^1	0	2.1 ± 1.1
% Q^0	0	0.09 ± 0.3

TABLE 3. Fraction of nbo and distribution of Q^n for our simulated 30:70 sodium silicate glass structure, compared to experimental glass with similar composition (22.5:77.5 sodium silicate).

c) Angular distribution

Another useful metric is the distribution of bond angles in the glass, which is related to the ring structure. In crystalline quartz, all Si–O–Si bonds make an angle of 109.5°, within Si 6-memebered rings. In a silicate glass, especially with glass forming elements like Na, the ring structure is broken and larger and smaller rings are formed. These larger rings have larger Si–O–Si bond angles. Fig. 4 shows the average of all Si–O–Si bond angles in the glass structure, also averaged over the 300 K equilibration trajectory. The peak is at the expected angle ~150° for sodium silicate glass, with the large broadening typical for amorphous structures. Figure 5 shows the distribution of Si rings in the structure.

[6] M Pota, A Pedone, G Malavasi, C Durante, M Cocchi, and M C Menziani, Computational Materials Science 47, 739 (2010).
[7] J. Du and A. N. Cormack, Journal of Non-Crystalline Solids 351, 2263 (2005).
[8] F. Angeli, O. Villain, S. Schuller, S. Ispas, and T. Charpentier, Geochimica et Cosmochimica Acta 75, 2453 (2011).

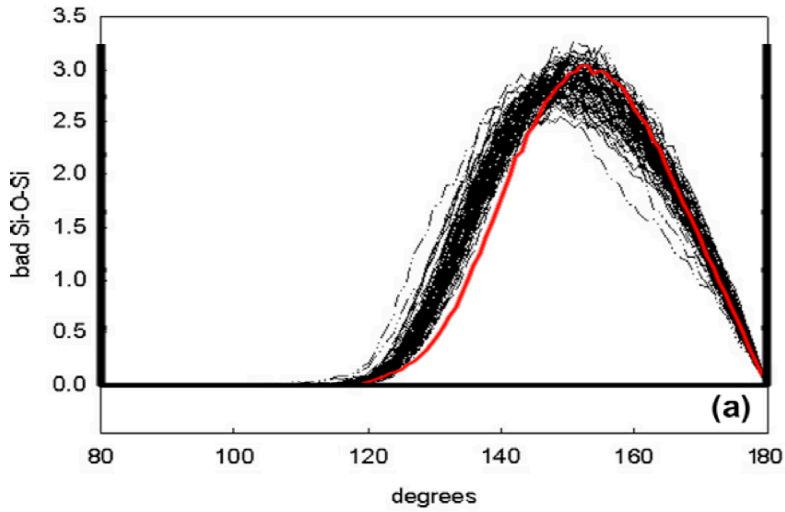

FIGURE 4. Si–O–Si bond angle distribution averaged over 50 equilibrated snapshots of the simulated E-glass 30:70 sodium silicate glass (thick red line), compared to an experimental ensemble of glass structures.[8]

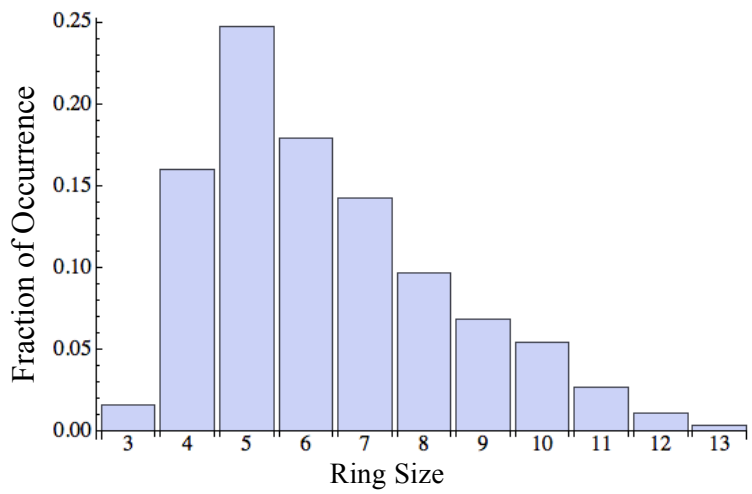

FIGURE 5. Distribution of Si ring sizes in the 30:70 sodium silicate glass model.

Electronic Structure

With a validated glass structure generated, we began to investigate the electronic structure, which is the ultimate goal. Nearly all of the 50 glass snapshots quenched from the 30:70 sodium silicate melt containing 648 atoms were relaxed using density functional theory with the PBE exchange-correlation functional using the VASP code. Due to the approximate nature of the empirical potential used to generate the glass structures, the atomic coordinates need to be relaxed within DFT. We perform the relaxation until all forces are below 0.05 eV/Å. Converged results are obtained using a 700 eV plane-wave cutoff and only the Γ point to sample the supercell Brillouin Zone. The nature of electronic states around the band gap region (band tail states, gap states, mobility edge states, etc.), their localization, and correlation to structural features of the glass can be extracted from the DFT calculations. The first set of results, which are not yet fully analyzed and compiled, is shown here.

The electronic densities of states from each snapshot are plotted in Fig. 6. A number of states within the gap are seen for each snapshot. An ensemble average of these DOS is more representative of the

electronic states of a macroscopic sample, but requires alignment of the energy scales of each snapshot; we are working to automate the alignment and ensemble averaging procedure and will report those results next quarter.

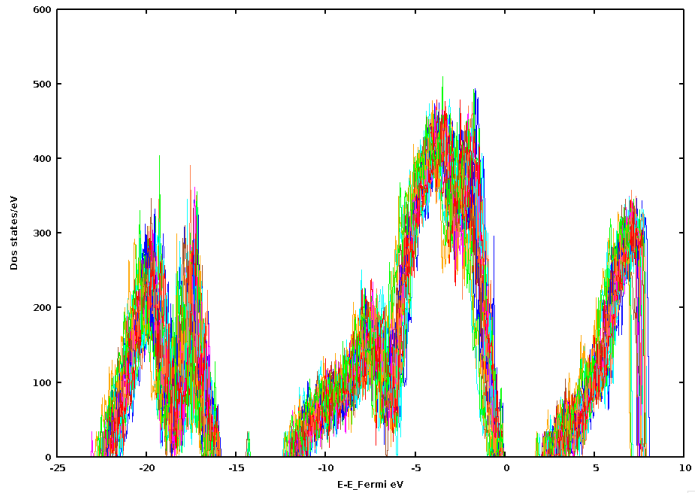

FIGURE 6. Electronic density of states of 50 snapshots of 30:70 sodium silicate glass containing 648 atoms after relaxation with DFT. The nominal VBM is set at 0.0 eV for each snapshot, but the variations of occupied gap states in each snapshot requires the energy scales to be individually shifted to align the "true" VBM.

The localization of states will be analyzed using the inverse participation ratio (IPR), which is a good measure of the spatial localization of a function. Here, we compute the IPR for each Kohn-Sham state ψ corresponding to energies around the band gap region. The IPR is defined as

$$I(\psi_n) = N \frac{\sum_{i=1}^{N} \left|\psi_n(\vec{r}_i)\right|^4}{\left[\sum_{i=1}^{N} \left|\psi_n(\vec{r}_i)\right|^2\right]^2}$$

A large value of IPR denotes a localized state (trap state), while a value near 1 denotes a completely delocalized (conduction) state. To compute all of the IPR values, a large number of partial charge density distributions must be generated, each of which is mapped onto a real-space grid whose spacing is dictated by the plane-wave cutoff. To speed up this large number of calculations, after convergence, we remap the total charge density onto a sparser grid using a 400 eV plane-wave cutoff. Figure 7 shows a range of ~200 calculated IPR, demonstrating no loss in fidelity by remapping to the sparser charge density grid. The data is Fig. 7 are illustrative, as they are not yet correlated with specific energy states around the band gap region or with structural features of the glass. Such analysis will be a focus in the next quarter.

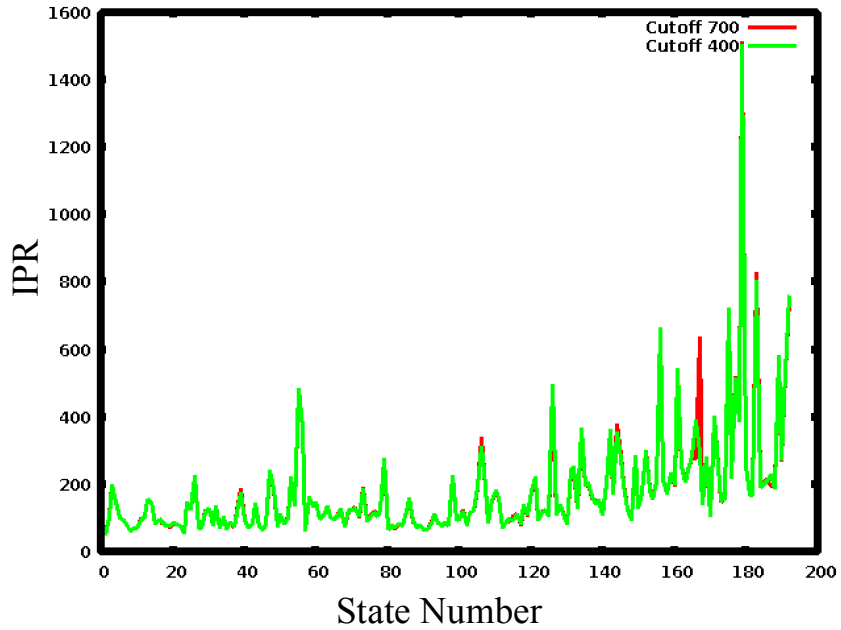

FIGURE 7. IPR values for a subset of energy states near the band gap from one snapshot of 30:70 sodium silicate glass. Red and green lines compare the results using charge densities mapped onto a grid corresponding to 700 eV and 400 eV plane-wave cutoffs, respectively.

Task 3: Build and determine electronic structure of various straight dislocations in CdTe

Upcoming and recent milestones/deliverables:
01/31/2014 — Obtain electronic gap states of a single straight edge dislocation, as a function of distance from the core
03/30/2014 — Use empirical potentials combined with density functional theory to generate structures and determine the electronic states of a set of at least 6 dislocations in CdTe
06/30/2014 — Submit manuscript on atomic and electronic structure of straight dislocations in CdTe to a peer-reviewed journal

All calculations and analysis for this task were completed last quarter, as planned. During this quarter, we presented the results at the Materials Research Society Spring Meeting on April 22, 2014. We also submitted an extended abstract to the Nuclear Science Symposium/Room-Temperature Semiconductor Detector Workshop describing our work and results. These documents are attached.

COMMENTS (BY TASK):

We made an offer for a new postdoc hire for the TlBr tasks (Keith Ray from UC Berkeley, who is currently a post-doc and former graduate student in Prof. Mark Asta's group). We anticipate a start date for Dr. Ray in Q3, to coincide with increased planned activities for Task 1.

In addition, we have accepted a summer graduate student (Chris Olson from North Dakota State University) to contribute to a portion of Task 2 from June 9 to August 16, 2014 (mostly during Q4). His focus will be on a parametric study of different melt-quench generation procedures for glass models representing the space of experimental variation in glass synthesis.

Planned work for next quarter is as follows.

Task 1: Build atomistic chemical models of TlBr–metal interface

In the next quarter we will continue our analysis of the TlBrCl alloy by explicitly treating the Cl composition dependence of the electronic properties. We will also continue working to construct a mechanistic model for how TlBr detector longevity may be improved by chlorinating the surface, including further investigating kinetic effects of atom and vacancy migration associated with chlorinated

layers. In addition, we will begin the study of compounds that may form by chemical reaction of different contact metals with TlBr.

Task 2: Generate atomistic models for two glass hosts

The focus of work next quarter will be to complete the electronic structure analysis (DOS and IPR) of the 3:7 sodium silicate glass. Alignment of the DOS to obtain an ensemble average will performed. The calculation of IPR from all relevant states in all 50 snapshots will be completed and also mapped onto the energy of states in the DOS. Finally, correlations between the electronic features and atomic structural features ("defects") in the glass will be developed, enabling a better understanding of carrier transport routes and mechanisms in the glass and how process/structure may influence them.

COSTING:

Costing information in webPMIS is current. Spending progress is on par against the cost plan.

MERIT REVIEWED PUBLICATIONS/TECHNICAL REPORTS/OTHER PUBLICATIONS:

V. Lordi, D. Åberg, M. Skarlinksi, and E. Cho, "Atomic and Electronic Structure of Dislocations in CdTe," H1.10, presented at the Materials Research Society Spring Meeting, San Francisco, Apr 22, 2014. (LLNL-PRES-653734)

V. Lordi, D. Åberg, M. Skarlinksi, and E. Cho, "Atomic and Electronic Structure of Dislocations in Cd(Zn)Te," extended abstract for Nuclear Science Symposium & Room-Temperature Semiconductor Detector Workshop, Seattle, Nov. 10-14, 2014. (LLNL-ABS-65318)

V. Lordi, N. Adelstein, D. Åberg, J. Varley, V. Bulatov, WMS 2014 Program Review poster, May 21, 2014. (LLNL-POST-654152)

OFFICE OF DEFENSE NUCLEAR NONPROLIFERATION RESEARCH & DEVELOPMENT

QUARTERLY PROGRESS REPORT FOR THE PERIOD JULY – SEPTEMBER 2014

PROJECT TITLE: Materials Modeling for High-Performance Radiation Detectors

webPMIS PROJECT NUMBER: LL13-MatModelRadDetect-PD2Jf LAB/CONTRACTOR: LLNL

B&R CODE: NN2001-02 DATE: October 3, 2014

PRINCIPAL INVESTIGATOR:	Vincenzo Lordi, 925-423-2755
LLNL PROJECT MANAGER:	Stephen A. Payne, 925-423-0570
LLNL POINT OF CONTACT:	Jenni Pruneda, 925-422-3037
HQ TEAM LEAD:	David B. Beach, 202-586-0346
HQ OFFICE MANAGER:	David A. LaGraffe, 202-586-1928

PROGRESS (BY TASK) DURING QUARTER:

Task 1: Build atomistic chemical models of TlBr–metal interface

Upcoming milestones:
09/30/2014 — Complete construction of atomistic interface model for 1 relevant metal

During this quarter, we focused on two aspects of the TlBr contact surface, partly motivated by work of our experimental collaborators at LLNL and RMD (DNDO project PI: A. Conway). The first continues our work from Q3 on TlBrCl alloys on the surface formed through chemical chlorination by etching with HCl. The second begins our study of possible interphase compounds formed between the contact metal and TlBr. This latter task seeks to more accurately describe the material stack at the contact, which may evolve over time, possibly driven by reactions of the metal with the semiconductor. The thermodynamics of these possible phases dictate which ones may form under different conditions. The relevant properties of interest of any stable phases include their band offsets, their diffusive properties (for vacancy and/or impurity injection), and the presence of charge traps in the bulk or at the interface, although this list is not exhaustive.

For the first sub-task, this quarter we completed the computational analysis of the band offsets of the TlBrCl alloy compared to pure TlBr, across the whole Cl composition range. We used special quasirandom structures (SQS) to model the random alloying of Cl into TlBr every 12.5% from 0 to 100% Cl. (In fact, we also compared to simpler models of ordered compounds at the same concentrations and found no significant effect of ordering on the band edge positions.) All calculations used the HSE hybrid functional for highest accuracy. First, we computed the band gap as a function of composition. We find a parabolic band bowing of 0.47 eV, with most of the increase in band gap with the additional of Cl occurring for Cl content greater than 40% (see Fig. 1a). Then, we computed valence band offsets using alternating slab models of TlBr/TlBrCl for compositions every 25%. (Tests showed that for these calculations, explicit slab models produced more reliable results than “branching point energy” calculations based on the charge neutrality point of impurity H in the supercells, which we have been able to use successfully in similar contexts in the past.) By combining with the band gap results, we can obtain the conduction band offsets as well. The results, when combined with experimental data (discussed

below), yield the variations of the band edges with Cl composition as shown in Fig. 1b. Most of the band gap bowing is found to occur in the conduction band edge and the variation of the valence band edge with composition is nearly linear. We also find that the absolute conduction band position does not vary much with Cl composition, remaining within ~0.1 eV over the entire composition range.

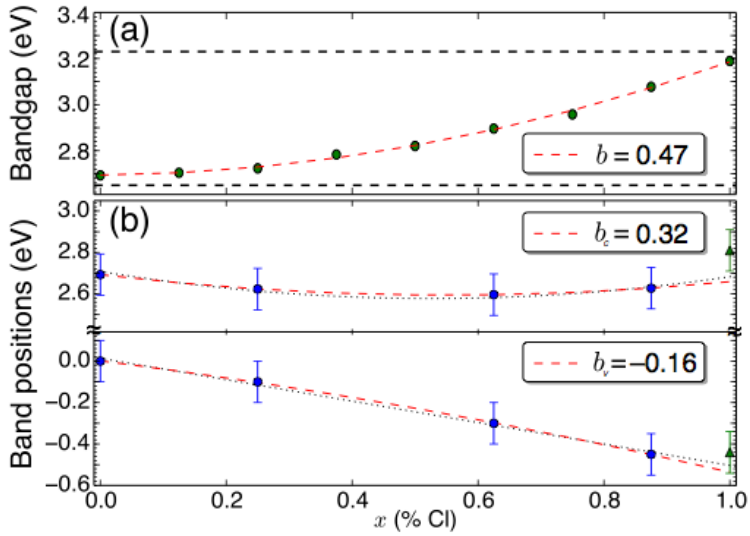

FIGURE 1. (a) Calculated variation of band gap of $TlBr_{1-x}Cl_x$ alloy as a function of composition, with the bowing parameter b indicated. (b) Dependence of conduction band edge (top panel) and valence band edge (bottom panel) on Cl composition, with respective band edge bowing parameters b_c and b_v indicated. The figure summarizes both experimental and theoretical data.

We were able to compare our results to recent experimental data, and in fact use our theoretical calculations to refine the measurement results to below the instrument energy resolution. XPS spectra were obtained from a series of TlBr samples exposed to different HCl etching treatments (Fig. 2). The surface compositions of the chlorinated materials were measured using relative intensities of Tl and Br core level XPS spectra (not shown) and also cross-checked with SIMS. Valence band spectra, referenced to *in situ* Cu and Au standards, allow the position of the VBM to be determined for each sample. However, instrument resolution is limited by the 0.85 eV linewidth of the Al Kα benchtop X-ray source used as well as a 0.1–0.3 eV detector energy resolution. Determining the precise position of the VBM thus requires extrapolation of the leading edge of the measured spectra, which can give good relative measure of the band offsets, but may also be complicated by variations of spectral shape with composition, as is the case here. In Fig. 2 can be seen a shoulder in the valence band spectra near the VBM that appears more prominent with increased Cl content. Calculations of the bulk valence band density of states for models of corresponding concentrations as the measurements show the development of such as shoulder, stemming from shifts in spectral features due to Br and Cl as the concentration varies. When broadened to simulate the energy resolution of the experimental apparatus, the theoretical DOS produce simulated valence band spectra in excellent agreement with the measured spectral shapes. By aligning the broadened theoretical DOS with the measured spectra, we can extract the precise positions of the VBM referenced to the experimental standard by using the theoretical values of the VBM, which are known to better than ~0.1–0.2 eV. This procedure also removes the uncertainly of the absolute offset of the extrapolated experimental data from the true VBM, which turns out to be on the order of a not insignificant 0.4 eV. Thus, we could extract the VBO across the composition range to an accuracy much higher than the nominal XPS instrument resolution would allow. The extracted results are those plotted in Fig. 1. We have submitted a manuscript together with our experimental collaborators describing this work, which is attached to this report.

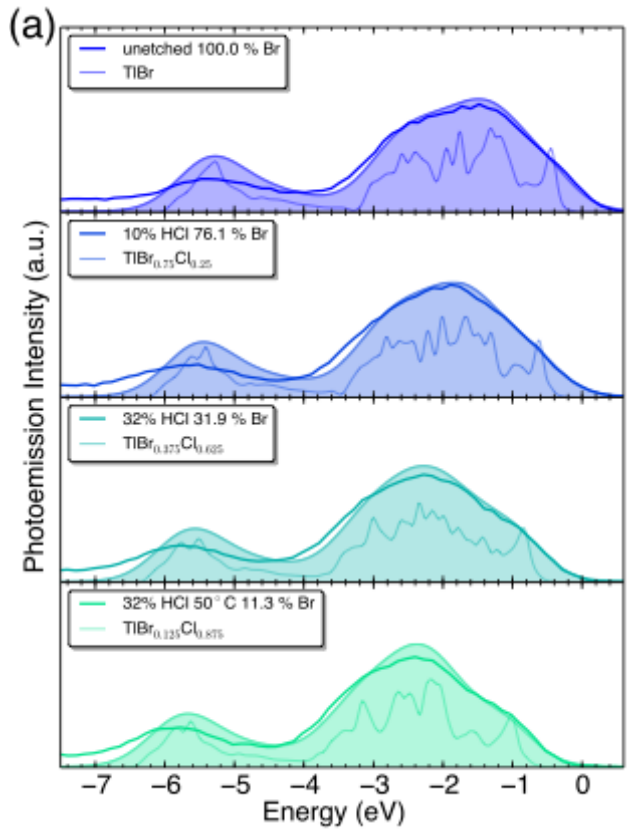

FIGURE 2. Experimental XPS data (thick lines) overlaid with calculated valence band density of states (thin lines) for different alloy compositions of TlBrCl, as indicated. The shaded regions are theoretical DOS broadened to match the instrument resolution. Subtle changes in the shape of the DOS near the VBM as the Cl concentration varies are reflected in the XPS data, allowing for very accurate determination of the measured band edges when fit with the theoretical spectra, to less than 0.2 eV accuracy (below instrument resolution).

During this quarter, we also began a thermodynamic assessment of possible interphase compounds forming between different metals and TlBr, work which will continue in later quarters. In later quarters, we also will investigate the various properties of interest of the discovered stable phases; we have not addressed these questions yet in the current quarter.

We began by assessing all known compounds in the Materials Project Database for the ternary phase spaces consisting of Tl-Br-*M* and Tl-Cl-*M* for 9 different metals *M* (Ag, Pb, Sn, Cr, Au, Ti, Pt, Ni, Bi). The metals were chosen from our prior work on metal contact impurities in TlBr. We also expanded our study of TlBr-compounds to TlCl-compounds, commensurate with our other work described above that suggests favorable device behavior with chlorinated material between TlBr and the metal contacts. From this search, we found many possible *M*-Br or *M*-Cl compounds to investigate; in addition, Pb and Sn were found to have stable ternary compounds of Tl-Br(Cl)-*M*, while Au and Pt have stable Tl-Cl-*M* compounds.

To begin our study, we generated model structures for the known Pt, Bi, and Ni compounds, since our prior work and the prior work of our experimental collaborators have suggested these to be among the highest performing metal contacts. Our work this quarter has focused on computing the relative thermodynamic stabilities of these compounds compared to TlBr(Cl) and solid *M*, to understand the conditions (temperature, electrical bias) under which they may form. This is ongoing work. In the near longer term, we plan to compute the band offsets and migration barriers for impurity motion through these phases in upcoming quarters.

Task 2: Generate atomistic models for two glass hosts

Upcoming and recent milestones/deliverables:
02/15/2014 — Construction of first complete glass model
03/30/2014 — Analysis of structure factor of model and comparison to experimental data from literature
08/30/2014 — Completion of two comparative glass models
09/30/2014 — Deliver report contrasting atomic structure motifs of two glass models and validation data to NA-22

Last quarter we completed the validation of the potential used to create the sodium silicate glass models, established the structure analysis tools, and generated structures. This quarter we focused on completing the calculations and analysis of the electronic structure of the generated glass, which included inventing a novel analysis correlating local structural features with electronic properties.

For our analysis, we sampled 30 configurations ("snapshots") from the 30:70 sodium silicate melt at 8000 K. Each sample was quenched to 300 K and annealed, as described last quarter, then relaxed at 0 K with DFT-PBE to extract the electronic structure. Various detailed analyses of each snapshot were performed, but here we report mainly results averaged across all snapshots, to best describe a bulk volume of glass. The shaded blue curve in Fig. 3 shows the averaged electronic density of states (DOS), after aligning all of the individual energy scales to match the deep states near –20 eV.

The energy between the highest occupied defect state and the lowest unoccupied state is about 1.5 eV. However, this is not to be considered the band gap of the material, as these states are associated with defects within the mobility gap (in addition to the normal band gap underestimate by PBE). The defect states in the gap are localized to various degrees, which we quantify using the inverse participation ratio (IPR) metric, discussed later.

The first peak below the VBM in the DOS is primarily from localized non-bridging oxygen (NBO) defect states. For our 30:70 glass, this peak is larger than for tetrasilicate (20:80) glass in the literature, which is expected since the higher sodium content in our glass results in more NBO defects. In addition, the tetrasilicate glass has a distinct peak near the conduction band minimum (CBM), while the band tail near the CBM in our calculation is more spread out.

To analyze the spatial localization, and consequent trapping character, of each state near the band edges, the IPR is calculated from the projected partial charge density of each Kohn-Sham state ("bands"). A large value of IPR indicates a very localized state, while values near unity are completely delocalized conduction or mobility states. This analysis can help quantitatively distinguish the localized band tail states from the mobility edges. The IPRs of all the bands near the VBM are plotted as dots on top of the DOS in Fig. 3, which shows that localized defects extend at least 3 eV below the nominal VBM, with a general trend of more localized states toward higher energies. The states near the bottom of the CBM are in general more delocalized and not included in Fig. 3 for clarity.

The character of each state can be determined by calculating its projection onto atomic orbitals. This also allows us to correlate each state with a structural feature, as follows. The top of the valence band is predominantly O-2*p* in character, and the localized defects near the VBM are often associated with non-bridging oxygen atoms. We characterize an NBO atom by the Q^n value of the Si to which it is bonded. In this way, we have color coded the IPR values plotted in Fig. 3, associating each state with a Q^n structural characteristic: Q^4 is green, Q^3 is blue, Q^2 is pink, Q^1 is yellow. Qualitatively, we observe that as the Q^n number decreases, the localization and energy of the defect increases. This is more easily seen in the histograms of the IPR values, as a function of energy, plotted below the *x*-axis in Fig. 3. The yellow Q^1 distribution is seen to be peaked highest in energy, followed by the pink Q^2, the blue Q^3, and finally the green Q^4. The distributions are not uniform and also overlap, indicating the variations of this general trend.

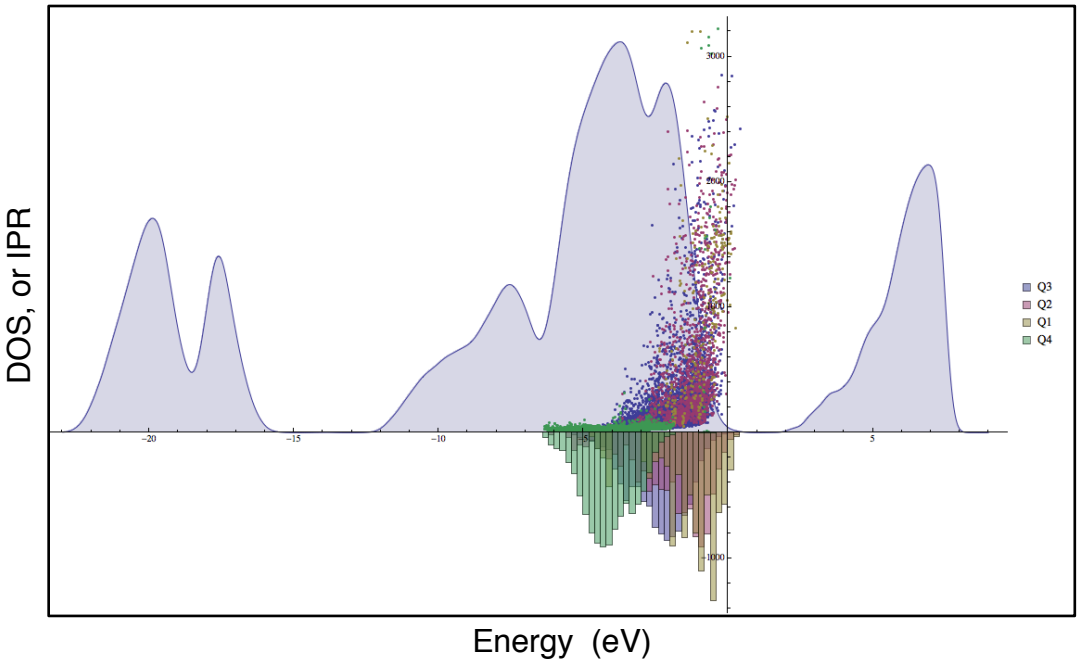

FIGURE 3. Averaged electronic DOS over 30 snapshots of 3:7 sodium silicate glass (blue shaded curve). The IPR of each state near the VBM is plotted with colored dots, coded by the Q^n-number character of the state (color given by key at right). Histograms of all the IPR values are plotted below the axis.

For comparison, an example analysis of a single snapshot is shown in Fig. 4. Here, we see the DOS near the VBM for a single snapshot (black line), along with various partial DOS (colored lines). The IPR values are plotted as brown symbols, showing the general trend of increased localization toward the top of the valence band, with significant localization starting around 1.5–2.0 eV below the nominal VBM. The red symbols plot the predominant Q^n value of each state (1 to 4). In this particular snapshot, we see that Q^1 states dominate the band edge, followed by a mixture of Q^2 and Q^3, and higher values of Q^n characterizing the delocalized states deeper in the DOS. The general trend is similar to the total result in Fig. 3.

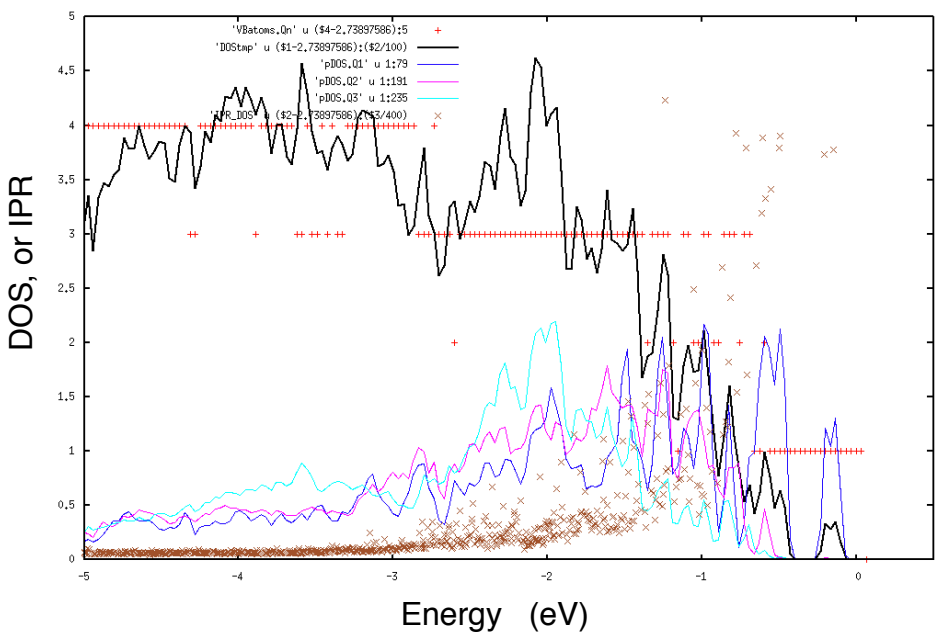

FIGURE 4. Total (black line) and partial (colored lines) DOS from a single snapshot of 3:7 sodium silicate glass. Brown symbols plot the IPR of each state, similarly to Fig. 3, with the predominant Q^n character of each state plotted as red symbols.

Finally, we can analyze the defect states directly in terms of localization by re-plotting the distribution of states on an IPR (localization) scale, as in Fig. 5, which shows histograms of each state within 6 eV of the Fermi level associated with a given Q^n value over IPR. Here, we see clearly that states are more localized when associated with Q^1 or Q^2 oxygen atoms compared to Q^3 or Q^4. The spread of the IPR values associated with Q^4 oxygens is very narrow, at low values that indicate very delocalized states. On the other hand, states associated with Q^1 or Q^2 oxygens have a wide spread and cover very large (very localized) IPR values. The distribution for Q^3 is in between. These results are integrated over all the states, irrespective of energy, so clearly show the correlation of localization of states and Q^n structural character. The distribution in Fig. 3 indicates their locations and spreads as a function of energy.

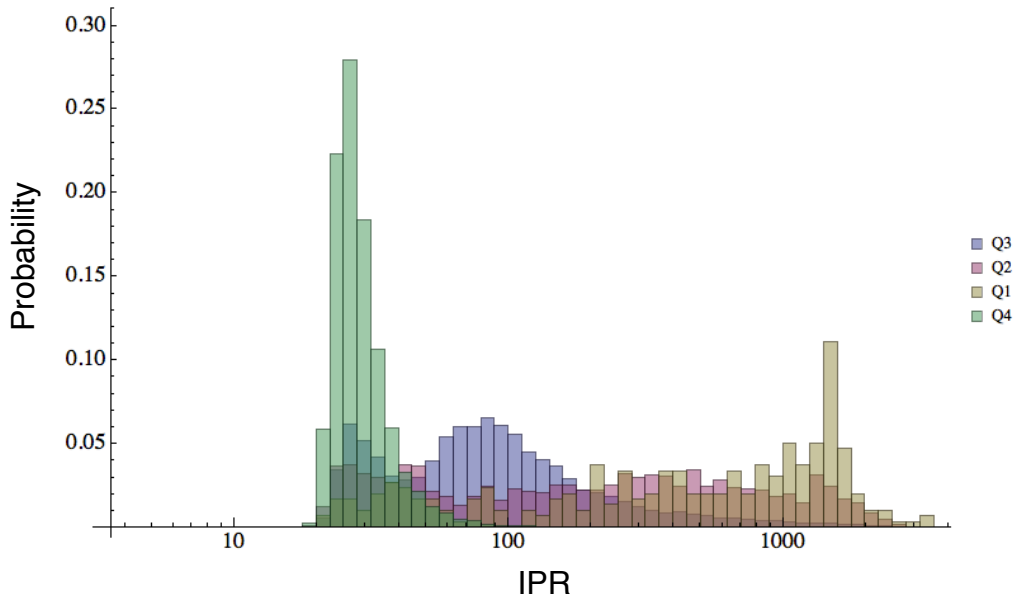

FIGURE 5. Histogram of IPR values, separated by Q^n, for 3:7 sodium silicate glass.

In summary, we calculated the electronic structure of 30:70 sodium silicate glass, using an ensemble of 30 configurations. Our analysis gives a detailed view of the localization and character of states near the band edges, beyond what has been previously done. In general, we find that NBO introduced by the incorporation of alkali ions (Na) into silicate glass can create many highly localized hole traps near the VBM, with the propensity for trapping correlated with increased local structural perturbation characterized by increased numbers of NBO (lower Q^n number).

In addition to the work above, a summer student (C. Olson) worked on investigation of the variation of glass structure by perturbing the melt-quench-anneal parameters over a wide range of values. The general result is that relatively small structural changes result even from large changes in the glass generation parameters, although significantly distinct structures are possible. The resulting glass structure, however, is much more sensitive to the potential parameters than the melt-quench-anneal parameters. The attached poster summarizes this work in additional detail.

COMMENTS (BY TASK):

Keith Ray, the new postdoc hired for the TlBr-related tasks, began work at LLNL on August 18. We are considering an additional postdoc hire to focus on future CdTe dislocation-related tasks and to assist with the TlBr effort. During this quarter, we conducted 3 phone/WebEx remote interviews of strong candidates from the Univ. of Texas as Austin and the Univ. of Pennsylvania. We selected one candidate for an onsite interview next quarter (in October 2014), for possible start around January 2015 (FY15 Q2).

Planned work for next quarter is as follows (relevant FY15 tasks identified):

Task 1: Build atomistic chemical models of TlBr–metal interface

We will continue calculations on the thermodynamic, electronic, and kinetic properties of various metal-TlBrCl compounds over the next quarters, as described above.

Task 2: Generate atomistic models for two glass hosts
Task 5: Compare electronic structure motifs in different glass hosts

Work on these tasks in the following quarters will focus on applying the established analysis framework to additional glass compositions and comparing the structural/electronic properties between them. The goal is to assess metrics for predicting better performing scintillator hosts.

Task 6: Build and determine electronic structure of kinked screw dislocation in CdTe

Over the next two quarters, we will continue the CdTe dislocation work by exploring the electronic structure of a kinked screw dislocation. We have already found that a straight screw dislocation does not introduce significant gap states, but a kink may trap charge. We will use empirical potentials to generate an atomistic model of the kinked dislocation in FY15 Q1. The model will be considerably larger than the models used for the straight dislocations, since additional unit cells are required along the line direction. We will subsequently (FY15 Q2) leverage the highly scalable DFT code qb@ll, which runs efficiently on up to several 100,000's of cores on the vulcan/sequoia BG/Q supercomputer at LLNL, to compute the electronic density of states.

COSTING:

Costing information in webPMIS is current. Spending progress is on par against the cost plan.

MERIT REVIEWED PUBLICATIONS/TECHNICAL REPORTS/OTHER PUBLICATIONS:

J.B. Varley, A.M. Conway, L.F. Voss, E. Swanberg, R.T. Graff, R.J. Nikolic, S.A. Payne, V. Lordi, and A.J. Nelson, "Effect of chlorination on the TlBr band gap for improved room temperature radiation detectors," submitted to *Physical Review B.* (LLNL-JRNL-661938)

C. Olson, N. Adelstein, and V. Lordi, "Defect Control in Silicate Glasses: Insights from Classical and Ab-Initio Simulations," poster presented at Computational Chemistry & Materials Science Summer Institute Student Poster Symposium, LLNL, Aug. 7, 2014. (LLNL-POST-658293)